MAGMATIC ORIGIN FOR SEDIMENT-HOSTED Au DEPOSITS, GUIZHOU PROVINCE, CHINA: IN SITU CHEMISTRY AND SULFUR ISOTOPE COMPOSITION OF PYRITES, SHUIYINDONG AND JINFENG DEPOSITS

Zhuojun Xie,[1] Yong Xia,[1,†] Jean S. Cline,[2] Michael J. Pribil,[3] Alan Koenig,[3] Qinping Tan,[1]
Dongtian Wei,[4] Zepeng Wang,[5] and Jun Yan[6]

[1] *State Key Laboratory of Ore Deposit Geochemistry, Institute of Geochemistry, Chinese Academy of Sciences, Guiyang, Guizhou Province 550081, China*

[2] *University of Nevada Las Vegas, Las Vegas, Nevada 89154, USA*

[3] *U.S. Geological Survey, Denver, Colorado 80225, USA*

[4] *Guilin University of Technology, Guilin 541004, China*

[5] *No. 105 Geological Team, Guizhou Bureau of Geology and Mineral Exploration and Development, Guiyang 550018, China*

[6] *Guizhou Institute of Technology, Guiyang 550002, China*

Abstract

The southwest Guizhou Province, China, contains numerous sediment-hosted Au deposits with Au reserves greater than 700 tonnes. To date, the source of ore fluids that formed the Guizhou sediment-hosted Au deposits is controversial, hampering the formulation of genetic models. In this study, we selected the Shuiyindong and Jinfeng Au deposits, the largest strata-bound and fault-controlled deposits in Guizhou, respectively, for detailed research on pyrite chemistry and S isotope composition using laser ablation-inductively coupled plasma-mass spectrometry (LA-ICP-MS) and laser ablation-multicollector-inductively coupled plasma-mass spectrometry (LA-MC-ICP-MS), respectively.

Petrography and pyrite chemistry studies distinguished five generations of pyrite. Among these, pre-ore pyrite 2 and ore pyrite are the most abundant types in the deposits. Pre-ore pyrite 2 is anhedral to euhedral and with ~2,639 ppm As and wider ranges of Cu, Sb, and Pb (<~22–4,837 ppm, <~6 to 532 ppm, and <~4 to 1,344 ppm, respectively). Gold in pre-ore pyrite 2 is below the detection limit of LA-ICP-MS (~2 ppm). Pre-ore pyrite 2 is interpreted to have a sedimentary (syngenetic or diagenetic) origin. Ore pyrite commonly rims the four identified pre-ore pyrites or occurs as individual, anhedral to euhedral crystals. Ore pyrite is enriched in Au (~641 ppm), As (~9,147 ppm), Cu (~1,043 ppm), Sb (~188 ppm), Hg (~43 ppm), and Tl (~22 ppm) in both deposits. Ore pyrite formed mainly by sulfidation of Fe in Fe-bearing host rocks, mainly Fe dolomite, and As, Cu, Sb, Hg, and Tl, also in ore fluids, were incorporated into ore pyrite.

In situ $\delta^{34}S$ isotope ratios for pre-ore pyrite 2 and ore pyrite were measured by LA-MC-ICP-MS. Pre-ore pyrite 2 from Shuiyindong and Jinfeng deposits resulted in $\delta^{34}S$ values ranging from –0.8 to +3.4‰ and from 5.1 to 10.5‰, respectively. Analyses of ore pyrite from the Shuiyindong have $\delta^{34}S$ values that vary from –3.3 to +2.5‰, with a median of 0.7‰; analyses of ore pyrite from the Jinfeng range from 8.9 to 11.2‰, with a median at 10.3‰. Available bulk and in situ $\delta^{34}S$ data in the literature for pre-ore pyrites 1 and 2 and ore-related sulfide minerals including ore pyrite, arsenopyrite, and late ore-stage stibnite, realgar, orpiment, and cinnabar from several Guizhou sediment-hosted Au deposits were compiled for comparison. Pre-ore-stage pyrites from Guizhou sediment-hosted Au deposits have a broad range of $\delta^{34}S$ values, from –33.8 to +17.9‰ (including in situ and available bulk $\delta^{34}S$ data). Ore-related sulfide minerals in all Guizhou sediment-hosted Au deposits, except Jinfeng, have very similar $\delta^{34}S$ values, and most data plot between ~–5 and +5‰. In the Jinfeng deposit, the ore-related sulfide minerals exhibit $\delta^{34}S$ values ranging from 1.9 to 18.1‰, with most data plotting between 6 and 12‰.

The broad range of S isotope compositions for the sedimentary pyrites (pre-ore pyrites 1 and 2) indicate that S in these pre-ore pyrites was most likely generated by bacterial reduction from marine sulfate. The narrow range of $\delta^{34}S$ values (~–5–+5‰) for ore-related sulfide minerals in all Guizhou sediment-hosted Au deposits, excepting the Jinfeng deposit, suggests that the deposits may have formed in response to a single widespread metallogenic event. As the S isotope fractionation between hydrothermal fluids and sulfide minerals in a sulfide-dominated system is small (<2‰) at ~250°C, the initial ore fluids that formed the Guizhou sediment-hosted Au deposits would have had $\delta^{34}S$ values similar to the ore-related sulfide minerals, between ~–5 and +5‰. At Jinfeng, initial ore fluids may have mixed with local fluids with heavier $\delta^{34}S$, possibly basin brine ($\delta^{34}S_{basin\ brine} >18‰$), resulting in elevated $\delta^{34}S$ values of ore-related sulfide minerals and especially late ore-stage sulfide minerals.

Although few igneous rocks are exposed in the mining area around these deposits, there is evidence of magmatic activity ~20 km away. Furthermore, gravity and magnetic geophysical investigations indicate the presence of a pluton ~5 km below the surface of the Shuiyindong district. Based on in situ S isotope results and recent data indicating proximal intrusions, we interpret a deep magmatic S source for the ore fluids that formed the Guizhou sediment-hosted Au deposits. However, as the age for Au mineralization of Guizhou sediment-hosted Au deposits is still debated, the mineralization-magma connection remains hypothetical. Identifying an ore fluid source and time frame for Guizhou Au mineralization continues to be a critically important research goal for this district.

†Corresponding author: e-mail, xiayong@vip.gyig.ac.cn

Introduction

One of the most significant characteristics of sediment-hosted Au deposits in the Youjiang Basin, Guizhou Province (from here on referred to as Guizhou deposits), is the consistent presence of invisible Au in arsenian pyrite (Hu et al., 2002, 2017; Zhang et al., 2003; Chen et al., 2009; Su et al., 2012; Hou et al., 2016; Xie et al., 2017, 2018; Yan et al., 2018)—a characteristic similar to the Nevada Carlin-type Au deposits (Arehart, 1996; Simon et al., 1999; Hofstra and Cline, 2000; Kesler et al., 2003, 2005; Cline et al., 2005; Reich et al., 2005; Muntean et al., 2011). These Au-bearing arsenian pyrites are also enriched in Sb, Hg, Tl, and Cu, interpreted to have been transported with Au in ore fluids and incorporated into Au-bearing pyrite (Simon et al., 1999; Hofstra and Cline, 2000; Cline et al., 2005; Su et al., 2009; Muntean et al., 2011; Tan et al., 2015a; Xie et al., 2017, 2018). Gold in these trace element-enriched ore fluids is interpreted to have been transported by S, most likely as a bisulfide complex ($Au(HS)^0$ and/or $Au(HS)_2^-$) (Seward, 1973, 1991; Stefánsson and Seward, 2004; Cline et al., 2005; William-Jones et al., 2009; Liu et al., 2014). Thus, the S isotope composition and the chemistry of the ore pyrites are key to better understanding the source of Au and ore fluids, ore fluid chemistry, and ore deposit genesis.

Previous studies of Guizhou sediment-hosted Au deposits resulted in two end-member models based on sources of ore fluids: (1) basin fluids enriched in ore-forming elements precipitated metals during sedimentation-diagenesis (Liu and Liu, 1997; Liu et al., 2001; Wang et al., 2002); (2) ore fluids liberated by deep metamorphic dehydration or magmatism ascended along regional faults and precipitated metals in sedimentary rocks (Liu et al., 2008; Su et al., 2009; Xia et al., 2009; Hu et al., 2017). Sulfur isotope analyses provide key data in discriminating between geologic models for these deposits. Sulfur isotope analyses of ore pyrite in some studies were conducted on physical separates of pre-ore and ore-stage pyrites, and these studies produced a broad range of S isotope ratios (see fig. 2 in Hou et al., 2016, and fig. 13 in Hu et al., 2017). However, sample purity may have been compromised by physical separation of the fine-grained pyrites, contributing to a wide range of S isotope values.

Recent advances including laser ablation-multicollector-inductively coupled plasma-mass spectrometry (LA-MC-ICP-MS), sensitive high-resolution ion microprobe (SHRIMP), and nanoscale secondary ion mass spectroscopy (nanoSIMS) now allow in situ analyses to distinguish trace elements and S isotope compositions between ore pyrite and pre-ore pyrite (Kesler et al., 2005; Large et al., 2007, 2009; Chang et al., 2008; Barker et al., 2009; Hou et al., 2016; Wei, 2017; Zheng, 2017; Yan et al., 2018). Hou et al. (2016) quantified S isotope ratios in various pyrite types from the Shuiyindong deposit using SHRIMP and determined that ore pyrite has a narrow range of $\delta^{34}S$ values (–1.2–+1.5‰). Wei (2017) and Zheng (2017) used LA-MC-ICP-MS to analyze the S isotope compositions of various pyrite types from the Nibao deposit and determined that ore pyrite has $\delta^{34}S$ values between –3 and 1‰. Furthermore, Yan et al. (2018) reported nanoSIMS S isotope analyses of various pyrite types from Jinfeng and demonstrated that the $\delta^{34}S$ of ore-pyrite inner rims ranged from 1.1 to 7.9‰. These studies indicate that S isotope data

collected using in situ techniques provide a narrow, consistent range of data for ore pyrites from several Guizhou sediment-hosted Au deposits. These results further suggest a similar S source for all Guizhou sediment-hosted Au deposits.

In this study, we present in situ trace element and S isotope data for pre-ore and ore pyrites using LA-ICP-MS and LA-MC-ICP-MS, respectively, from the Shuiyindong and Jinfeng deposits. For comparison, we compiled available $\delta^{34}S$ data for pre-ore pyrites and ore-related sulfide minerals including ore pyrite, ore- and late ore-stage arsenopyrite, and late ore-stage stibnite, realgar, orpiment, and cinnabar from other Guizhou sediment-hosted Au deposits. To date, the ore-related sulfide minerals from Guizhou sediment-hosted Au deposits have $\delta^{34}S$ values primarily from ~–5 to +5‰, consistent with a magmatic S source.

Geology of Guizhou Sediment-Hosted Au Deposits

Key deposit characteristics

Almost all Guizhou sediment-hosted Au deposits are located within the Youjiang Basin (Fig. 1), and the unique characteristics distinguishing the deposits include the following. (1) Signature ore elements include Au, As, Cu, Sb, Hg, and Tl with low to absent Ag and base metals. (2) Orebodies are preferentially hosted by carbonate-bearing rocks and are controlled by faults and/or anticlines, and (3) most Au is ionically bound in trace element-rich, subhedral-euhedral arsenian pyrite, though minor arsenopyrite contains trace Au (Zhang et al., 2003; Xia, 2005; Chen et al., 2009; Xia et al., 2009; Su et al., 2012; Tan, 2015; Hou et al., 2016; Xie et al., 2017, 2018). These Au-bearing sulfide minerals are commonly disseminated in variably altered host rocks. (4) The most important and consistently present alteration features spatially associated with Au-bearing ore pyrite include dissolution of calcite, jasperoid replacement of calcite, and sulfidation of Fe in Fe dolomite to form Au-bearing pyrite and dolomite. Variable additional alteration includes minor illite replacement of K-feldspar/muscovite and formation of minor vein quartz (Zhang et al., 2003; Peters et al., 2007; Cline et al., 2013; Tan et al., 2015a; Su et al., 2018; Xie et al., 2018). The observed alteration, especially calcite dissolution and formation of dolomite during the ore stage, is consistent with ore formation from near-neutral (pH ~5.5) ore fluids (Xie et al., 2017, 2018). (5) Stibnite, realgar, calcite, quartz, and lesser orpiment and cinnabar precipitated in open space within veins during the late ore stage, and these veins crosscut and/or are near orebodies (Tan et al., 2015b; Xie et al., 2018). In addition, (6) the deposits generally formed at depths between 2 and 8 km and at temperatures of 190° to 300°C (average ~250°C) from low-salinity (<5 wt % NaCl equiv) and CO_2-rich (6–75 mole %) reduced fluids (Zhang et al., 2003; Wang et al., 2013a; Su et al., 2009, 2018). No known coeval porphyry, skarn, or distal Ag-Pb-Zn mineralization has been identified near the deposits.

Geologic setting

The tectonic setting of the Youjiang Basin summarized by Xie et al. (2018) is briefly described here. Extension commenced from Early Devonian passive margin rifting along the southwestern margin of the Precambrian Yangtze craton, which produced a series of high-angle normal faults that
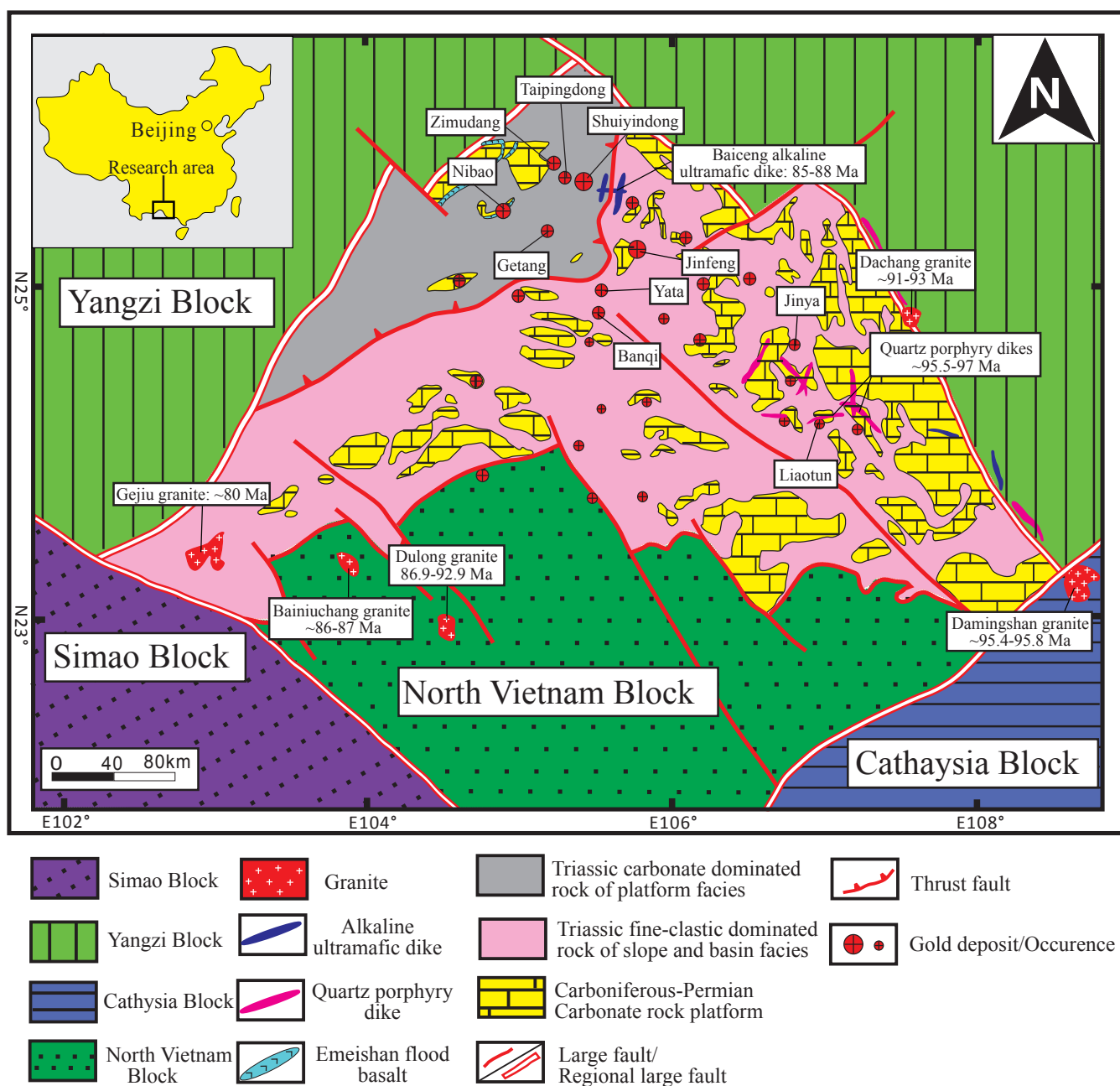
Fig. 1. Regional geologic map showing the distribution of sediment-hosted Au deposits in the Yunnan-Guizhou-Guangxi "golden triangle" region (modified from Chen et al., 2011; Xie et al., 2018). The Youjiang Basin consists of Triassic carbonate-dominated rock of platform facies (gray) and Triassic fine, clastic-dominated rock of slope and basin facies (pink). Sources for dates are as follows: Baiceng alkaline ultramafic dikes, LA-ICP-MS zircon U-Pb and phlogopite ^{40}Ar/^{39}Ar, Liu et al., 2010; quartz porphyry dikes, SIMS and LA-ICP-MS zircon U-Pb, Zhu et al., 2017; Gejiu granite, SHRIMP and LA-ICP-MS zircon U-Pb, Cheng and Mao, 2010; Bainiuchang granite, LA-ICP-MS zircon U-Pb, Cheng et al., 2010; Dulong granite, SHRIMP zircon U-Pb, Liu et al., 2007; Damingshan granite, molybdenite Re-Os, Li et al., 2008; and Dachang granite, zircon SHRIMP U-Pb, Cai et al., 2006.

shaped the Youjiang Basin and subsequently controlled sedimentation and deformation (Bureau of Geology and Mineral Resources of Guangxi Zhuang Autonomous Region, 1985; Hu et al., 2002; Chen et al., 2011). Subsequent to rifting and from the Devonian to Triassic, a passive margin sequence developed on the continental margin. In the northwestern part of the Youjiang Basin, a sequence of shallow-water platform-facies sedimentary rocks mainly consisting of carbonate rocks interbedded with terrigenous detrital rocks formed (gray unit, Fig. 1; Wang, 1990; Han et al., 1999). In the southern and eastern part of the basin, deeper-water slope/basin-facies sedimentary rocks, which are dominated by calcareous mudstone, siltstone, and siliceous rocks interbedded with thinly layered carbonate rock and sandstone,

were deposited (pink unit, Fig. 1; Wang, 1990; Han et al., 1999). Following passive margin deposition, two subduction events including subduction of the Pacific plate and of the Meso-Tethys Ocean may have influenced the magmatism and deformation of the Youjiang Basin. Li and Li (2007) suggested that W-verging subduction of the Pacific plate beneath the Eurasian plate (Hilde et al., 1977; John et al., 1990) during the mid-Permian folded the basin sequence (see fig. 4, Li and Li, 2007). Alternatively, Lai et al. (2014) and Zaw et al. (2014) proposed that the NE-verging subduction of the Meso-Tethys Ocean beneath Sibumasu began during the Early Cretaceous (see fig. 11, Zaw et al., 2014) and caused the Late Triassic intracontinental deformation of Youjiang Basin.

Several igneous rocks including granites, quartz porphyry dikes, and alkaline ultramafic dikes are exposed in the Youjiang Basin (Fig. 1). In the west, east, and southeast parts of the basin (Fig. 1), granites are exposed (~80–95.6 Ma, Cai et al., 2006; Liu et al., 2007; Li et al., 2008; Cheng and Mao, 2010; Cheng et al., 2010; Mao et al., 2013; Xu et al., 2015), which are interpreted as mainly derived from crustal melts that intruded the sedimentary rocks. Some of these intrusions contributed to the formation of polymetallic tin/tungsten deposits (Mao et al., 2013). Minor quartz porphyry dikes (95–97 Ma, Chen et al., 2014; Zhu et al., 2017) and alkaline ultramafic dikes (85–88 Ma, Liu et al., 2010) related to the onset of basin extension intruded the sedimentary rocks. Most of these dikes are ~10 to 30 km from the sediment-hosted Au deposits (Fig. 1). Only at the Liaotun Au deposit in the southeastern part of the Youjiang Basin is there an unaltered quartz porphyry dike that crosscuts the Au orebody (Fig. 1; Chen et al., 2014).

To date, the mineralization age for Guizhou sediment-hosted Au deposits remains controversial because of the lack of minerals clearly related to Au mineralization that are suitable for dating (Hu et al., 2007). Su et al. (2018) and Xie et al. (2018) discuss ages proposed for Au mineralization using different methods and conclude that the most reliable proposed ages are based on crosscutting relationships. Chen et al. (2014) described an unaltered quartz porphyry dike crosscutting the orebodies at the Liaotun Au deposit (Fig. 1). An $^{40}Ar/^{39}Ar$ plateau age of 95.5 ± 0.7 Ma was determined for a magmatic muscovite phenocryst from this dike. This age provides a minimum value for Au mineralization. Wang (1997) identified a small Jurassic sedimentary rock exposure near the Shuiyindong and Jinfeng districts, which is conformable and folded with Late Triassic sedimentary rocks. Because some of the orebodies in the Shuiyindong and Jinfeng deposits crosscut these folds, Au mineralization should be synchronous with or younger than the folding, which suggests a maximum Jurassic age for Au mineralization. Collectively, these relationships indicate that the Au mineralization that formed the Guizhou sediment-hosted Au deposits occurred between Jurassic and Late Cretaceous time.

Geology of the Shuiyindong deposit

Currently, the Shuiyindong Au deposit consists of four ore blocks including Shuiyindong, Xionghuangyan, Bojitian, and Nayang. The combined deposit has Au reserves of 263 tonnes (t) (8.46 million ounces [Moz]), with an average Au grade of 5 g/t (0.16 oz/t), and is the largest sediment-hosted Au deposit

discovered to date in the Youjiang Basin (Tan, 2015). Su et al. (2018) and Xie et al. (2018) have described the geology of Shuiyindong deposit in detail. A brief summary follows.

The Shuiyindong deposit is controlled by the Huijiabao anticline, which is ~5 km wide and ~20 km long with both limbs dipping at low angles (Fig. 2). The strata-bound orebodies are mainly on the flanks and crest of the anticline (Fig. 2) and are principally hosted by the Upper Permian Longtan bioclastic limestone. The strata above and below the bioclastic orebodies are typically thick-bedded argillite. These impermeable layers promoted ore fluid reaction with bioclastic limestone, contributing to the formation of high-grade ore (locally Au >100 g/t). An unconformity between the Longtan and underlying Maokou Formation also hosts some low-grade strata-bound orebodies (Fig. 2). Tan et al. (2015a) proposed that this unconformity was the structural conduit that fed ore fluids into the anticline core (Tan et al., 2015a; Fig. 2).

Igneous rocks have not been identified by geologic mapping or drilling in the Shuiyindong district. The nearest igneous rocks, the Baiceng alkaline ultramafic dikes (85–88 Ma, Liu et al., 2010), are ~20 km from this deposit (Fig. 1). However, geophysical investigations (Bouguer gravity and magnetic surveys) indicate the presence of a pluton ~5 km below the surface at Shuiyindong (Liu, pers. commun., 2018).

Geology of the Jinfeng deposit

The Jinfeng deposit, the second largest sediment-hosted Au deposit in Guizhou, has proven and probable Au reserves of 57.9 t (1.86 Moz) with an average Au grade of 3.83 g/t (0.12 oz/t) (Eldorado Gold Corp., 2016), and ~51 t (1.64 Moz) of Au has been mined (Lu, pers. commun., 2018). The following geologic descriptions are summarized from Xie et al. (2018).

The stratigraphy at Jinfeng is divided into two distinct sequences with Au mineralization primarily in carbonaceous siltstone of the third and fourth subunits of the fourth unit of the Middle Triassic Xuman Formation (Xuman Formation 4-3, 4-4) and the Middle Triassic Bianyang Formation in the upper sequence (Fig. 3; Zhang et al., 2003; Chen et al., 2011; Chen et al., 2011). The Xuman Formation 4-3 (Fig. 3) has a thickness up to 250 m in the Jinfeng district and mainly consists of dolomitic siltstone and thick-bedded to massive calcareous mudstone with a few interlayered sandstone lenses. The Xuman Formation 4-4 is dominated by thick-bedded sandstone intercalated with argillite. The Bianyang Formation, which lies above the Xuman Formation, exceeds 300 m in thickness and consists largely of turbiditic sandstone, siltstone, and silty argillite.

The Jinfeng district underwent multiple periods of shortening and extension, which are characterized by reactivated faults (Chen et al., 2011). The F2 and F3 fault zones are the major ore-controlling structures, with the F3 fault zone controlling ~80% of Au reserves at Jinfeng (Fig. 3). The F3 fault zone, with an apparent normal sense of displacement, strikes north to northwest and dips steeply to the northeast (Fig. 3).

As in the Shuiyindong deposit, geologic mapping and drilling have yet to identify any igneous rocks in the Jinfeng district. The Baiceng alkaline ultramafic dikes (85–88 Ma, Liu et al., 2010) are the nearest igneous rocks and are ~20 km from this deposit (Fig. 1).
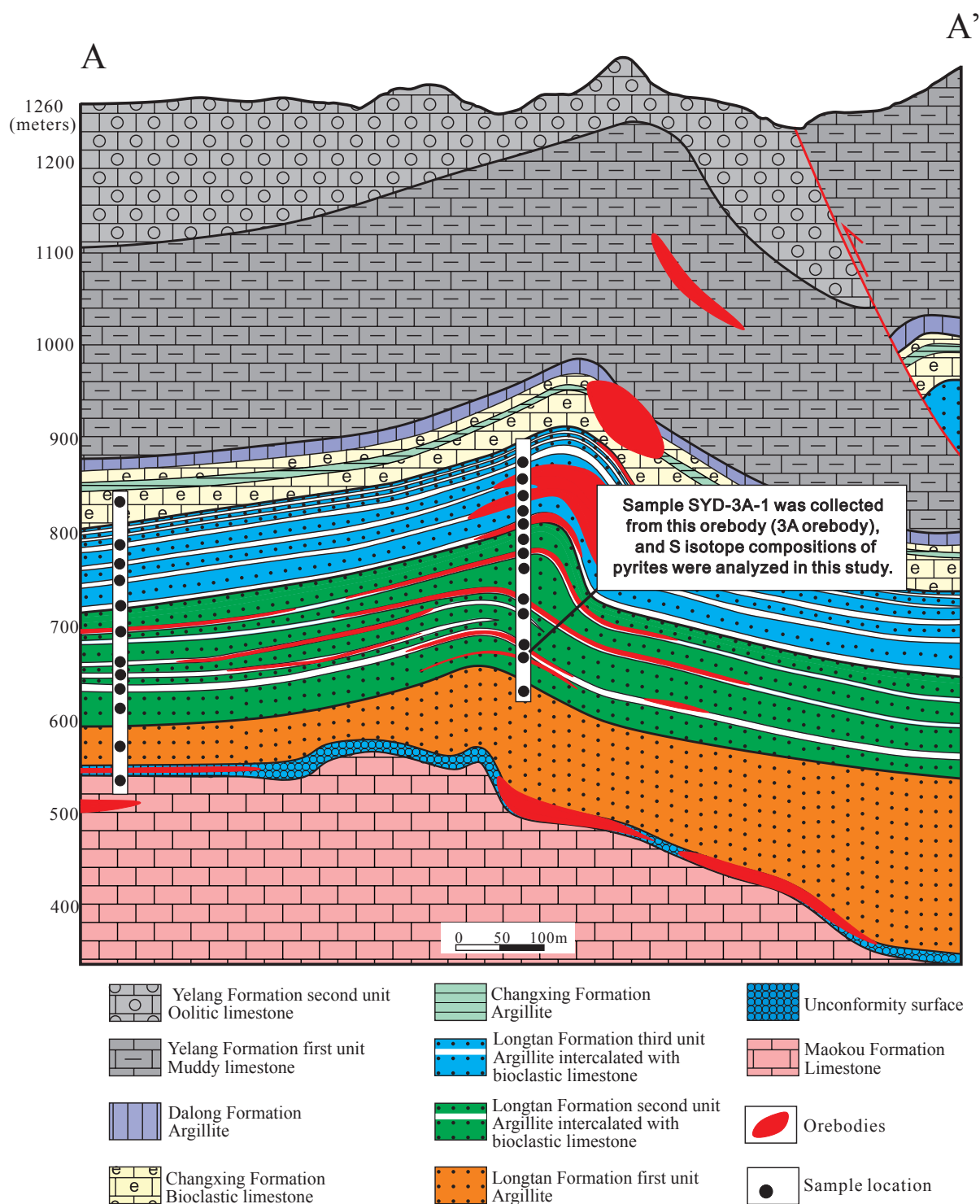
Fig. 2. Geologic cross section of the mineralized Huijiabao anticline in the Shuiyindong deposit, showing sample locations (modified from Tan et al., 2015a; Xie et al., 2018).

Methods

Pyrite morphology and texture

A total of ~289 samples were collected from the Shuiyindong and Jinfeng deposits, and 59 polished thin sections were prepared (Table 1). All sections were examined using transmitted and reflected light microscopy to identify mineralogy and to observe mineral morphology and texture. The JSM-5600 scanning electron microscope (SEM) and JSM-6700F field emission SEM at the University of Nevada Las Vegas (UNLV)

Fig. 3. Geologic cross section of the Jinfeng deposit, showing the transect sample locations (modified from Xie et al., 2018).

Table 1. Samples and Polished Sections Collected and Analyzed Using LA-ICP-MS and LA-MC-ICP-MS

| Deposits | No. of samples | Polished sections | LA-ICP-MS analysis | | | | LA-MC-ICP-MS sulfur isotope analysis | |
			Polished sections	Spots	Lines	Maps	Polished sections	Spots
Shuiyindong	167	29	7	90	7	5	1	51
Jinfeng	122	30	6	59	4	3	1	25

Electron Microanalysis and Imaging Laboratory (EMiL) were used to identify and confirm minerals and observe mineral morphology and texture, especially textures relating to pyrite. The JSM-6700F field emission SEM, with resolution reaching 10 nm, was optimized for imaging nanoscale minerals and textures, particularly of fine-grained pyrites and framboidal pyrites. High-resolution images were obtained to illustrate textures and provide precise locations for LA-ICP-MS and LA-MC-ICP-MS analyses.

In situ trace element analysis of pyrite

In situ trace element analyses of pyrites from 13 polished sections (Table 1) were conducted using LA-ICP-MS at the U.S. Geological Survey, Denver, Colorado. A Photon Machines Analyte G2 LA system (193 nm, 4-ns Excimer laser) was coupled to a PerkinElmer DRC-e inductively coupled plasma-mass spectrometer. The ablated material was carried to a modified glass mixing bulb by He carrier gas (0.8 l/min). To improve the efficiency of aerosol transport, the He carrier gas was mixed with Ar (0.6 l/min). Single-spot ablation was carried out using a 5-or 10-μm spot size at 3 J/cm^2. Line and map ablations were carried out using a 4- or 8-μm spot size at 4 J/cm^2. Scanning speed was 1 μm/s. Line analyses were ablated using 25 pulses/s (25 Hz). The protocol from Longerich et al. (1996) was used to calculate the concentration and detection limit, and the ^{57}Fe isotope was used as the internal standard for concentration calculations. Detection limits for these analyses are listed in Appendix 1.

In situ S isotope analysis of pyrite

The ^{34}S/^{32}S isotope ratios of pyrites in two samples (one from Shuiyindong [Fig. 2] and one from Jinfeng [Fig. 3]) were analyzed using LA-MC-ICP-MS at the U.S. Geological Survey, Denver, Colorado (Table 1). The procedure and operating conditions were described in detail by Pribil et al. (2015). Briefly, in situ ^{34}S/^{32}S isotope ratio measurements were performed using a Teledyne CETAC Photon Machines G2 Excimer laser ablation (LA) system coupled to a Nu Instruments HR® MC-ICP-MS. The instrument was operated in pseudo high-resolution mode to resolve polyatomic interferences from ^{16}O-^{16}O for ^{32}S, ^{32}S-^{1}H for ^{33}S, and ^{16}O-^{18}O for ^{34}S. Pyrite and reference material samples were analyzed using 20- to 60-μm spot sizes at a frequency of 5 to 10 Hz. The laser energy was 2.2 mJ, resulting in a fluence of 2 to 3 J/cm^2. The ablated sample material was transported from the LA system sample chamber using two mass flow controllers (MFC), with MFC 1 at an He gas flow rate of 0.400 l/min and MFC 2 at an He gas flow rate of 0.350 l/min. The LA system sample flow was introduced to the instrument using an LA gas mixing chamber with a makeup Ar gas flow rate of approximately 0.900 ml/min.

Time-resolved data acquisition mode was used to collect and integrate data. Each sample acquisition began by collecting an on-peak background for 30 s, followed by 30-s data acquisition. Typical background for ^{32}S ranged from 20 to 40 mV. All analyses followed standard-sample bracketing procedures of three samples bracketed by S isotope reference material.

A ZnS glass was used as the bracketing standard for the in situ analyses. This internal reference material was analyzed independently by the USGS light stable isotope lab (δ^{34}S = 0.78 ‰ ± 0.3) and cross-verified using NIST SRM 8554 (International Atomic Energy Agency [IAEA] S-1), resulting in a δ^{34}S of 0.81‰ ± 0.21 (Pribil et al., 2015).

Secondary sulfide reference materials were used to determine accuracy and precision. The error for the measurements is 0.21‰ 2 standard deviations (SD) based on secondary in-house sulfide reference materials. The $^{34/32}$S isotope ratios are reported in ‰ using a delta notation (δ) (Krouse and Coplen, 1997) reported relative to the Vienna-Canyon Diablo troilite (V-CDT) using the following expression:

$$\delta^{34}S_{V-CDT} = \left[\frac{\frac{34}{32}S_{sample}}{\frac{34}{32}S_{reference\ V-CDT}} - 1 \right] \times 1{,}000.$$

Results

Pyrite types

Based on pyrite morphology, texture, and chemistry, Xie et al. (2018) identified five distinct pyrites in both the Shuiyindong and Jinfeng deposits, including pre-ore pyrites 1, 2, 3, and 4, and ore pyrite (Fig. 4; Table 2). Pre-ore pyrites 1 and 2 dominate in low-/no-grade rocks and account for ~90% of the total pre-ore pyrites in both deposits. Pre-ore pyrites 3 and 4 locally occur in both deposits. Ore pyrite is the dominant pyrite in high-grade ore in both deposits. The following descriptions of pyrite types are summarized from Xie et al. (2018).

Pre-ore pyrite 1 is framboidal, consisting of ~0.5- to 3-μm-diameter pyrite crystallites separated by pore space (Fig. 4A; Table 2). Pre-ore pyrites 2, 3, and 4 are anhedral to euhedral pyrites (Fig. 4B, C; Table 2) and are indistinguishable under the microscope as they have a similar yellowish-white color, bright reflectivity, and high relief (Fig. 4B). However, they are chemically distinct and can be distinguished under backscattered electron (BSE) imaging; pre-ore pyrite 2 is darker than pre-ore pyrites 3 and 4 (Fig. 4C), probably because pre-ore pyrite 2 contains less As.

Ore pyrite commonly rims pre-ore pyrites, and rims are usually 5 to 30 μm thick (Fig. 4D- F). It also forms individual, anhedral to euhedral pyrite crystals, 5 to 30 μm in diameter. Chemical zoning displayed by pre-ore and ore pyrites
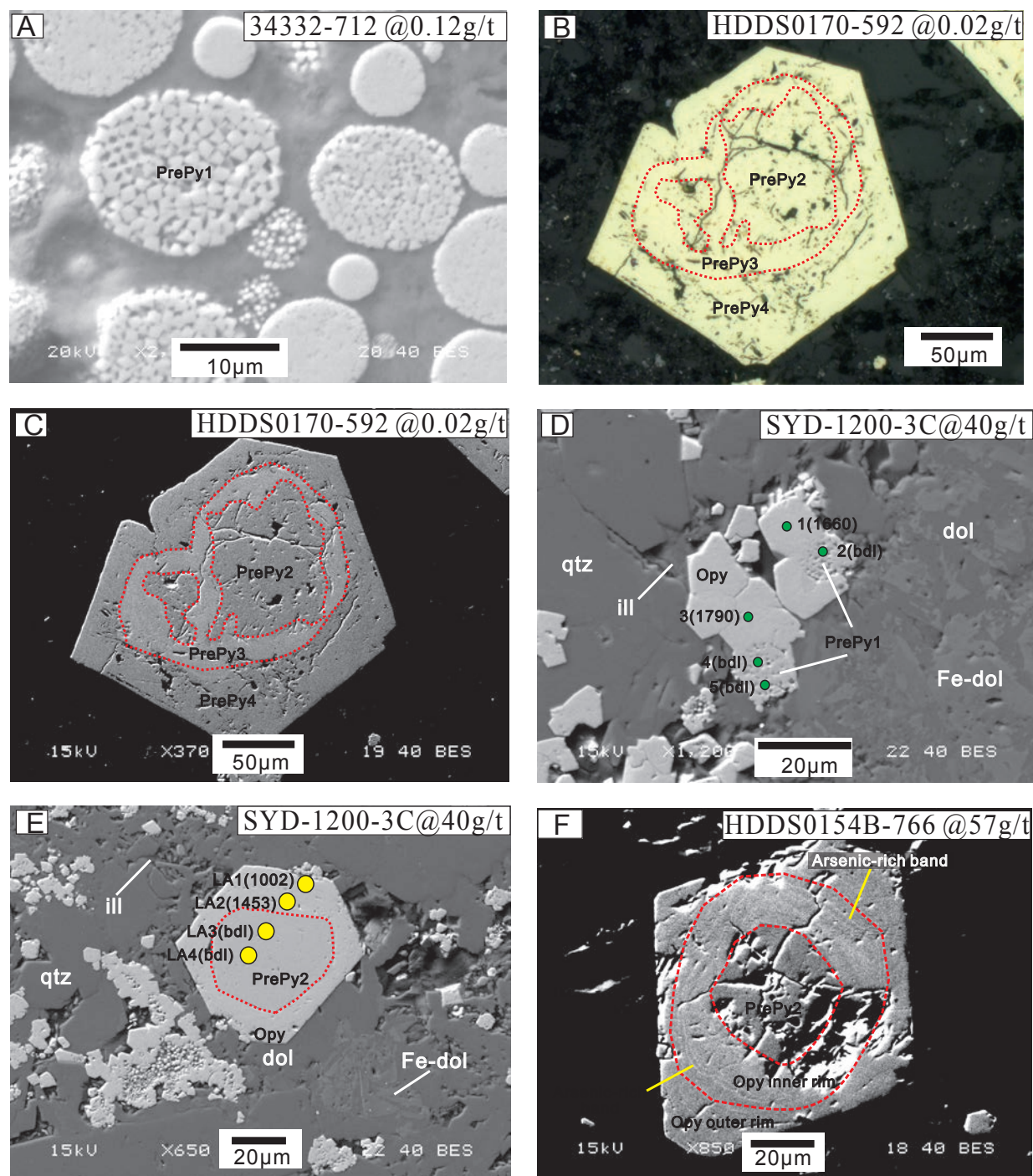
Fig. 4. Images of pyrite types from Shuiyindong (A, D, and E) and Jinfeng (B, C, and F). The label in the top right of images A to C and F indicates the sample number, consisting of drill hole number, sampling depth, and Au grade; the label in the top right of images D and E indicates the sample number and Au grade. A. Framboidal pyrite (pre-ore pyrite 1) consists of abundant euhedral pyrite crystallites and pore space (backscattered electron [BSE] image). B, C. Pre-ore pyrite 2 is rimmed by pre-ore pyrite 3, which is rimmed by pre-ore pyrite 4. Pre-ore pyrites 2 to 4 (B, reflected and transmitted crossed-polarized light) have a similar yellowish-white color, bright reflectivity, and high relief; however, pre-ore pyrite 3 (C), which contains more As than pre-ore pyrites 2 and 4, is brighter under BSE imaging at low brightness and high contrast. D. Framboidal pyrite (pre-ore pyrite 1; BSE) is rimmed by euhedral/subhedral ore pyrite. Green dots indicate locations of EPMA, and analysis numbers and Au concentration in ppm are shown. All EPMA data were listed in the appendix of Xie et al. (2018). E. Pre-ore pyrite 2 (BSE) is rimmed by ore pyrite, which has a similar morphology and high relief. Yellow dots indicate locations of LA-ICP-MS analyses, and analysis numbers and Au concentration in ppm are shown. All LA-ICP-MS data are listed in Table 4. F. Jinfeng ore pyrite inner rim has multiple As-rich subbands (BSE). Abbreviations: bdl = below detection limit (~2 ppm for LA-ICP-MS analyses, ~120 ppm for EPMA), dol = dolomite, Fe-dol = Fe dolomite, ill = illite, Opy = ore pyrite, PrePy1 = pre-ore pyrite 1, PrePy2 = pre-ore pyrite 2, PrePy3 = pre-ore pyrite 3, PrePy4 = pre-ore pyrite 4, qtz = quartz.

Table 2. Pyrite Classification for Shuiyindong and Jinfeng Deposits

Pyrite type	Stage	Morphology and spatially associated minerals	Chemistry	Sulfur isotope composition	Interpretation
PrePy1	Pre-ore stage	Yellowish white framboidal pyrite, consisting of 0.5- to 4-μm spherical or euhedral pyrite crystallites; occurs with calcite, Fe dolomite, and quartz; rimmed by ore pyrite in ore	Au bdl of LA-ICP-MS (~2 ppm), high Co (~635 ppm) and Ni (~1,328 ppm)	δ^{34}S values from –7.5 to +5.9‰ for Shuiyindong deposit (Hou et al., 2016)	Diagenetic/syngenetic
PrePy2	Pre-ore stage	Yellowish white, bright reflectivity, anhedral to subhedral, poor polish, commonly 5 to 50 μm in diameter; occurs with calcite, Fe dolomite, and quartz; rimmed by ore pyrite in ore	Au bdl of LA-ICP-MS, low As (~2,639 ppm), a wider range of trace element Cu, Sb, and Pb (<~22–4,837 ppm, <~6–532 ppm, and <~4–1,344 ppm, respectively)	δ^{34}S values from –0.8 to +3.4‰ for Shuiyindong deposit; δ^{34}S values between 5.1 and 10.5‰ for Jinfeng deposit (this study)	Diagenetic/syngenetic
PrePy3	Pre-ore stage	Yellowish white, euhedral to subhedral, good polish, bright reflectivity; occurs with calcite, Fe dolomite, quartz, and illite; rims PrePy2	Au bdl of LA-ICP-MS, high As (~13,848 ppm) and Cu (~495 ppm)	δ^{34}S values from –2.6 to +1.5‰ for Shuiyindong deposit (Hou et al., 2016)	Pre-ore high As and Cu hydrothermal fluid or early Au hydrothermal fluid
PrePy4	Pre-ore stage	Yellowish white, euhedral to subhedral, good polish, bright reflectivity; occurs with calcite, Fe dolomite, quartz, and illite; rims PrePy2 and PrePy3	Au bdl of LA-ICP-MS, moderate As (~2,009 ppm), and high Cu (~706 ppm)	Too small to analyze via LA-MC-ICP-MS	Pre-ore high-As and Cu hydrothermal fluid or early Au hydrothermal fluid
OPy	Ore stage	Yellowish white, bright reflectivity, good polish; occurs as euhedral to subhedral crystals or rims pre-ore pyrites; surrounded by jasperoid quartz, dolomite, and variable illite; note that in Jinfeng deposit the ore pyrite inner rim has multiple ~1- to 3-μm As-rich subbands	High Au (~641 ppm), high As (~9,147 ppm), enriched in Cu (~1,043 ppm), Sb (~188 ppm), Hg (~43 ppm), and Tl (~22 ppm); in Jinfeng, the ore pyrite inner rim, with multiple As-rich subbands, commonly contains lower Au but higher As and Cu than the ore pyrite outer rim	δ^{34}S values from –3.3 to +2.5‰ for Shuiyindong deposit (Hou et al., 2016; this study); δ^{34}S values from 1.1 to 18.1‰ for Jinfeng deposit (Yan et al., 2018; this study)	Au hydrothermal fluid

Modified from Xie et al., 2018
Abbreviations: bdl = below detection limit, OPy = ore pyrite, PrePy1 = pre-ore pyrite 1, PrePy2 = pre-ore pyrite 2, PrePy3 = pre-ore pyrite 3, PrePy4 = pre-ore pyrite 4

is apparent under BSE imaging adjusted for low brightness and high contrast (Fig. 4F). Note that in the Jinfeng deposit, the ore pyrite inner rim has multiple ~1- to 3-μm subbands with elevated As concentrations that are apparent under BSE imaging (Fig. 4F). The presence of subbands is rare in the Shuiyindong deposit. In addition, in the Jinfeng deposit, most individual pyrite types have subhedral to euhedral crystal faces; however, the boundaries between the various pyrite types within a crystal are locally highly irregular and generally rounded (Figs. 4C, F).

Pyrite geochemistry

The concentrations of trace elements in different pyrite types as determined by LA-ICP-MS are included in Appendix 2 and displayed in Figures 5 to 7. The average and median values of trace elements in each pyrite type from LA-ICP-MS analysis are listed in Table 3.

Pre-ore pyrite 1 contains high Co (average = 635 ppm) and Ni (average = 1,328 ppm), and low As (average = 1,283 ppm) compared to ore pyrite, which contains low Co (average = 136 ppm) and Ni (average = 198 ppm), and high As (average = 9,147 ppm) (Table 3; Fig. 5). Laser ablation-ICP-MS analysis did not detect any Au in pre-ore pyrite 1 (Table 3;

Fig. 5A). Pre-ore pyrite 2 has a wider range of trace element concentrations—especially Cu, below detection (~22 ppm) to 4,837 ppm; Sb, below detection (~6 ppm) to 532 ppm; and Pb, below detection (~4 ppm) to 1,344 ppm—compared to pre-ore pyrite 1 and ore pyrite (Fig. 5). Gold in pre-ore pyrite 2 is commonly below the detection limit of LA-ICP-MS (Tables 3, 4; Figs. 5A, 6A-C). Pre-ore pyrites 3 and 4 contain higher As (average = 13,848 and 2,009 ppm, respectively) and Cu (average = 495 and 706 ppm, respectively), compared to pre-ore pyrite 1. Gold in pre-ore pyrites 3 and 4 is commonly below the LA-ICP-MS detection limit (Table 3; Fig. 5A) and occasionally above the detection limit (Table 3; Fig. 5A).

Ore pyrite (Table 3, Fig. 5) contains ~641 ppm Au, ~9,147 ppm As, ~1,043 ppm Cu, ~188 ppm Sb, ~43 ppm Hg, and ~22 ppm Tl (Table 3), and ore pyrite is, in general, more enriched in these elements than the pre-ore pyrites (Figs. 5A-F, 6A-F, 7A-E, Table 4). However, in Jinfeng, the ore pyrite inner rim that exhibits multiple ~1- to 3-μm As-rich subbands (Figs. 4F, 7A) commonly contains lower Au but higher As and Cu than the ore pyrite outer rim (Fig. 7A-E; fig. 21 in Xie et al., 2018). A Spearman rank correlation matrix of ore pyrite was constructed using LA-ICP-MS
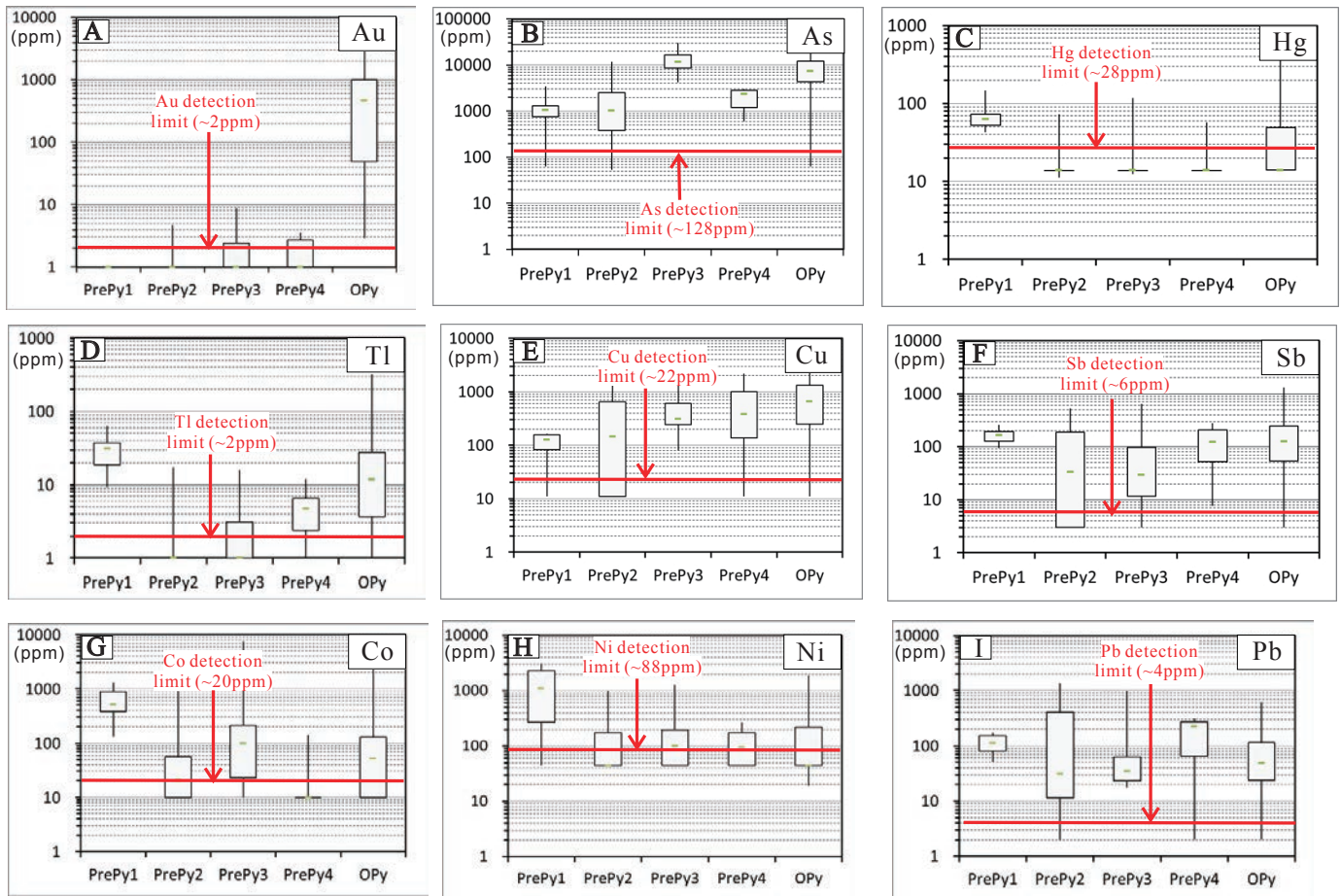
Fig. 5. Box-and-whisker diagrams showing LA-ICP-MS data (Appendix 2) for Au (A), As (B), Hg (C), Tl (D), Cu (E), Sb (F), Co (G), Ni (H), and Pb (I) in pre-ore and ore pyrites from both deposits. Detection limits are shown on the image. The bar indicates the median value, the box encompasses the 25th to 75th percentile of data, and the whiskers indicate the minimum and maximum values. Abbreviations: OPy = ore pyrite, PrePy1 = pre-ore pyrite 1, PrePy2 = pre-ore pyrite 2, PrePy3 = pre-ore pyrite 3, PrePy4 = pre-ore pyrite 4.

data (Appendix 2) and included in Appendix 3. Gold correlates positively (>0.4) with As (0.52), Tl (0.55), and Sb (0.6). Other strong positive correlations include As and Sb (0.53), Sb and Hg (0.65), Sb and Tl (0.65), Hg and Tl (0.44), Pb and Sb (0.8), Pb and Hg (0.53), Pb and As (0.42), and Pb and Tl (0.46).

Pyrite sulfur isotope compositions

In situ δ^{34}S values of pre-ore pyrite 2 and ore pyrite in two samples (one from Shuiyindong [Fig. 2] and one from Jinfeng [Fig. 3]) were quantified by LA-MC-ICP-MS analyses (Figs. 6A, H, 7H) and shown in Figure 8 and Table 5. Pre-ore pyrites 1, 3, and 4 are too small (commonly less than 20 μm in diameter, the minimum spot size of LA-MC-ICP-MS) to analyze using LA-MC-ICP-MS. Twenty-eight spots including 20 spots from Shuiyindong and eight spots from Jinfeng on pre-ore pyrite 2, and 48 spots including 31 spots from Shuiyindong and 17 spots from Jinfeng on ore pyrite were analyzed (Table 5). Pre-ore pyrite 2 sulfur isotopes for Shuiyindong and Jinfeng have δ^{34}S values from –0.8 to 3.4‰, and 5.1 to 10.5‰, respectively (Fig. 8; Table 5). In Jinfeng samples, pre-ore pyrite 2 is commonly ~20 to 40 μm in diameter (Fig. 7A, H) and LA-MC-ICP-MS spot

size ranges from 20 to 60 μm; thus, pre-ore pyrite 2 analyses from Jinfeng may have included some ore pyrite during analysis. Ore pyrite δ^{34}S values determined for Shuiyindong vary from –3.3 to +2.5‰, with a median of 0.7‰. Ore pyrite values for Jinfeng are markedly higher and range from 8.9 to 11.2‰, with a median at 10.3‰, ~10‰ greater than the median value of Shuiyindong ore pyrite (Fig. 8; Table 5). In the Shuiyindong sample, the pre-ore pyrite 2 core and ore pyrite rim exhibit δ^{34}S values that slightly decrease from pre-ore pyrite 2 to ore pyrite (Fig. 6A, H). In the Jinfeng sample, however, the pre-ore pyrite 2 core and ore pyrite rim have δ^{34}S values that slightly increase from pre-ore pyrite 2 to ore pyrite (Fig. 7H). Note that the Jinfeng ore pyrite inner rim commonly exhibits multiple ~1- to 3-μm As-rich bands that cannot be individually analyzed (Fig. 4F), and LA-MC-ICP-MS spots will average the values within a spot analysis.

Interpretation and Discussion

Pyrite formation

Pre-ore pyrite: Pre-ore pyrites 1 and 2 lack gold and are commonly rimmed by ore pyrite in the Shuiyindong and Jinfeng
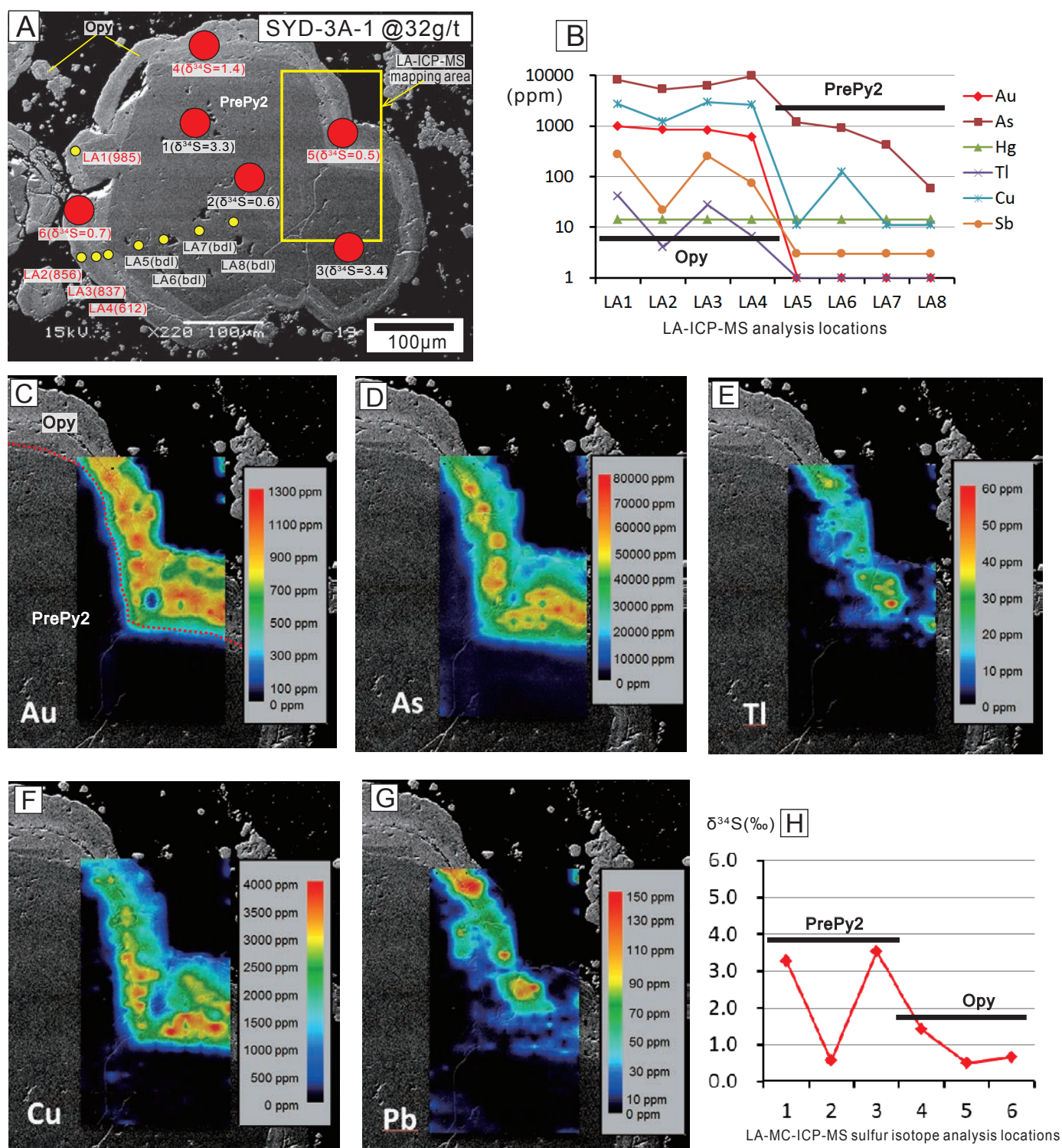
Fig. 6. Textural (A), chemistry (B-G), and δ^{34}S isotope composition (H) of pre-ore pyrite 2 and ore pyrite from the Shui-yindong deposit (sample SYD-3A-1, 32 g/t Au). A. Anhedral pre-ore pyrite 2 is rimmed by ore pyrite. Yellow and red dots indicate locations of LA-ICP-MS and LA-MC-ICP-MS analyses, respectively, and were marked with analysis number and Au concentration in ppm and δ^{34}S isotope composition in ‰, respectively. All LA-ICP-MS data are tabulated in Table 4. B. Spider diagram of LA-ICP-MS data shows ore pyrite contains more As, Tl, Cu, and Sb than pre-ore pyrite 2. C-G. LA-ICP-MS maps of Au (C), As (D), Tl (E), Cu (F), and Pb (G) showing the correlation of these elements in pre-ore pyrite 2 and ore pyrite; the pre-ore pyrite 2 core lacks these elements. H. Spider diagram of δ^{34}S isotope composition analyzed by LA-MC-ICP-MS, showing that δ^{34}S isotope compositions of pre-ore pyrite 2 are slightly greater than those of the ore pyrite. The lower δ^{34}S value for point 2 compared with points 1 and 3 could result from a mixture of ore and pre-ore pyrites. Abbreviations: bdl = below detection limit (~2 ppm for LA-ICP-MS analyses), OPy = ore pyrite, PrePy2 = pre-ore pyrite 2.
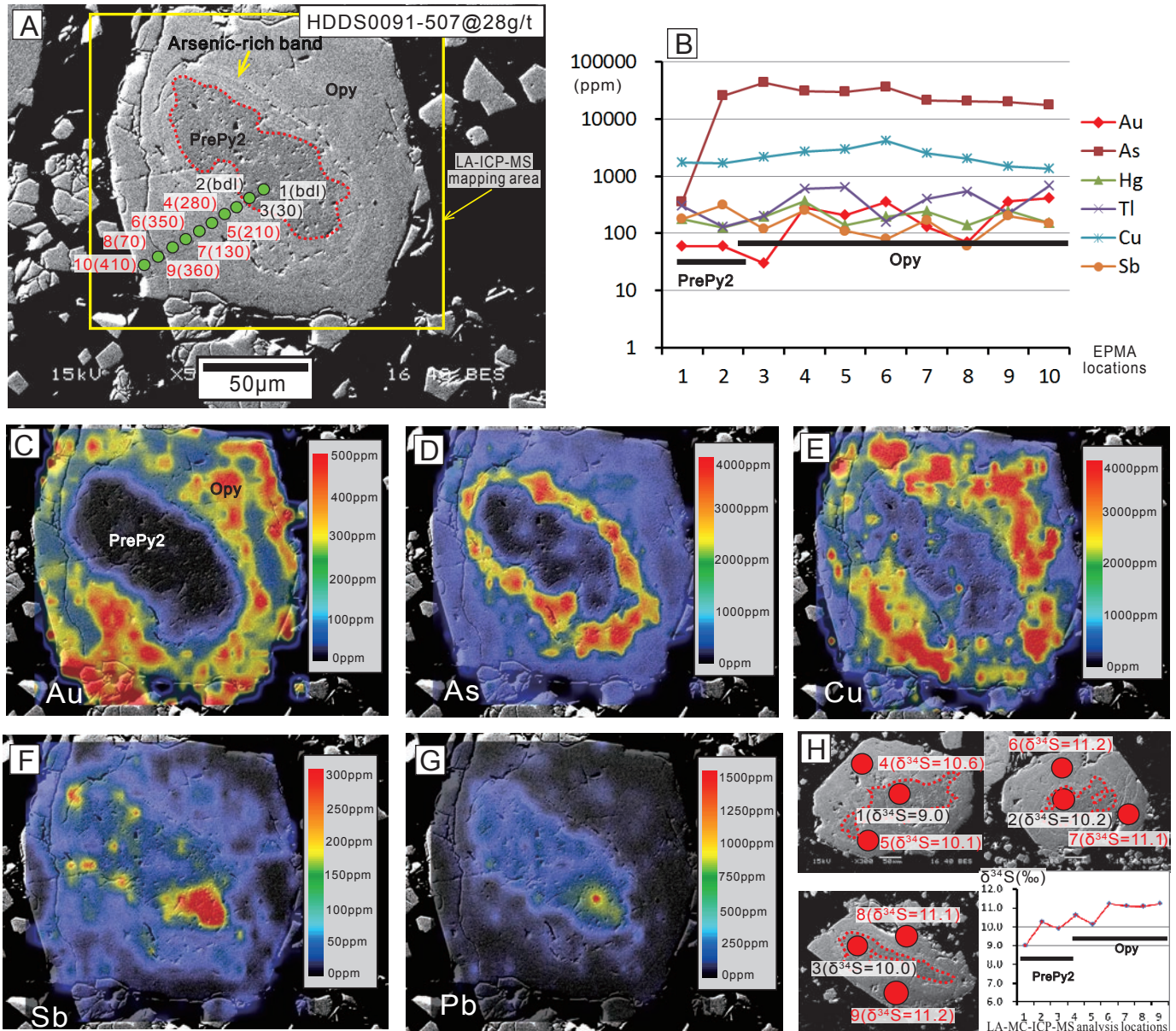
Fig. 7. Textural and BSE (A), chemistry (B-G), and $\delta^{34}S$ isotope composition (H) of pre-ore pyrite 2 and ore pyrite from the Jinfeng deposit (sample HDDS0091-507, 28 g/t Au). A. Anhedral pre-ore pyrite 2 is rimmed by ore pyrite. The inner rim of ore pyrite has As-rich subbands. Green dots are locations of EPMA spots. Labels show analysis number and Au concentration in ppm. All EPMA data were listed in the appendix of Xie et al. (2018). B. Spider diagrams of EPMA data show that ore pyrite contains more As, Au, and Tl than pre-ore pyrite 2. C-G. LA-ICP-MS maps of Au (C), As (D), Cu (E), Sb (F), and Pb (G) showing the correlation of these elements in pre-ore pyrite 2 and ore pyrite. The inner rim is more enriched in As and Cu than the outer rim. H. Three pre-ore pyrite 2 cores with ore pyrite rims (BSE images) and a spider diagram of $\delta^{34}S$ isotope compositions, analyzed by LA-MC-ICP-MS, of pre-ore pyrite 2 (spots 1–3). These compositions are generally lower than those of ore pyrite (spots 4–9). Red dots are locations of $\delta^{34}S$ analyses and isotopic compositions are in ‰. Abbreviations: bdl = below detection limit (~120 ppm for EPMA), Opy = ore pyrite, PrePy2 = pre-ore pyrite 2.

deposits, demonstrating that they formed before the ore pyrites. Large et al. (2009) and Gregory et al. (2015) analyzed global sedimentary pyrites and determined that they contain abundant As, Ni, Pb, Cu, and Co, and less abundant Mo, Sb, Zn, and Se. Pre-ore pyrites 1 and 2 exhibit textural and chemical similarities (Tables 2, 3) to these sedimentary pyrites, which is consistent with a sedimentary (syngenetic or diagenetic) origin (Xie et al., 2018). Pre-ore pyrites 3 and 4,

which contain high concentrations of As and Cu but no/low Au, could have precipitated during an Au-free but As- and Cu-rich period of the hydrothermal event or at the beginning of the ore stage from low-Au and As- and Cu-rich fluids (Xie et al., 2018).

Ore pyrite: Ore pyrite is the main ore mineral in the Shuiyindong and Jinfeng deposits, although minor arsenopyrite also contains trace Au in these deposits (Zhang et al., 2003;

Table 3. Average and Median Values (ppm) of Trace Elements in Each Type of Pyrite from LA-ICP-MS Analysis, Shuiyindong and Jinfeng Deposits

Pyrite type	Stage	No. of analyses	Au ~2[1]	As ~128[1]	Hg ~28[1]	Tl ~2[1]	Cu ~22[1]	Sb ~6[1]	Pb ~4[1]	Ni ~88[1]	Co ~20[1]	Sn ~30[1]	Ag ~10[1]	Mn ~42[1]	Zn ~210[1]
	Average value														
PrePy1	Pre-ore	N = 6	1	1,283	74	31	109	167	114	1,328	635	15	9	68	132
PrePy2	Pre-ore	N = 22	1	2,639	17	2	753	127	267	152	76	31	7	44	151
PrePy3	Pre-ore	N = 7	3	13,848	29	4	495	127	170	268	1,148	15	10	196	259
PrePy4	Pre-ore	N = 6	2	2,009	21	5	706	134	177	122	32	15	12	36	326
OPy	Ore	N = 109	641	9,147	43	22	1,043	188	98	198	136	20	9	58	207
	Median value														
PrePy1	Pre-ore	N = 6	1	1,051	62	31	125	166	112	1,086	504	15	7	71	105
PrePy2	Pre-ore	N = 22	1	1,018	14	1	146	34	31	44	20	15	5	21	105
PrePy3	Pre-ore	N = 7	1	11,631	14	1	307	29	34	99	99	15	5	21	105
PrePy4	Pre-ore	N = 6	1	2,334	14	5	381	123	224	95	10	15	5	32	105
OPy	Ore	N = 109	467	7,327	14	12	660	126	48	44	52	15	5	21	105

Notes: Data used to calculate the average and median values are listed in Appendix 2; we use half the detection limit if the analysis is below detection limit during average and median values calculation
Abbreviations: OPy = ore pyrite, PrePy1 = pre-ore pyrite 1, PrePy2 = pre-ore pyrite 2, PrePy3 = pre-ore pyrite 3, PrePy4 = pre-ore pyrite 4
[1]Value listed below the element is the approximate detection limit (in ppm)

Chen et al., 2009; Hou et al., 2016) and locally trace native Au was reported in Shuiyindong deposit (Su et al., 2008, 2012). Previous studies have suggested that the ore pyrite from Guizhou sediment-hosted Au deposits is similar to the ore pyrite from Nevada Carlin-type Au deposits, though the ore pyrite morphologies and trace element abundances differ in the Nevada and Guizhou deposits (Cline et al., 2013; Xie et al., 2018). Studies of the Nevada deposits are consistent with ore pyrite formation by sulfidation of host-rock Fe by fluids transporting Au, As, Hg, Tl, Cu, and Sb in addition to S to form Au and trace element-rich pyrite (Hofstra et al., 1991; Stenger et al., 1998; Kesler et al., 2003; Ye et al., 2003; Cline et al., 2005; Muntean et al., 2011; Maroun et al., 2017; Xie et al., 2018). Similarly to the Nevada ore pyrite, Guizhou ore pyrite is enriched in Au, As, Cu, Sb, Hg, and Tl. Ore-stage fluid inclusions from Shuiyindong, analyzed using LA-ICP-MS (Su et al., 2009), contain <~400 μg/g Fe, the detection limit for

Fe using this technique. These analyses are consistent with petrographic observations that increasing Au grade in Shuiyindong and Jinfeng ore correlates directly with consumption of Fe from spatially associated Fe dolomite and alteration of Fe dolomite to Fe-free dolomite (see fig. 25, Xie et al., 2018). Arsenic, Cu, Sb, Hg, and Tl were also incorporated into the ore pyrite during this sulfidation process. Locally, in Jinfeng, irregular boundaries between pre-ore and ore pyrites suggest that replacement in addition to sulfidation may have been important in the formation of ore pyrite (Xie et al., 2018).

One difference between ore pyrite in the Shuiyindong and Jinfeng deposits is that the Jinfeng ore pyrite inner rim commonly contains multiple As-rich subbands. This oscillatory variation in As concentration appears to have recorded fluctuations in the chemical composition of the ore fluids and may suggest ore fluid pulsing instead of a continuing influx in the Jinfeng district.

Table 4. LA-ICP-MS Analyses of Pyrites in Shuiyindong Deposit (ppm)

Analysis no.	Pyrite type	Au ~2[1]	As ~30[1]	Hg ~30[1]	Tl ~5[1]	Cu ~20[1]	Sb ~5[1]	Bi ~3[1]	Ag ~10[1]	V ~40[1]	Mn ~40[1]	Co ~20[1]	Ni ~50[1]	Pb ~4[1]	Zn ~210[1]	Sn ~30[1]	S ~20,000[1]
Figure 4E (SYD-1200-3C, 40 g/t, Shuiyindong deposit)																	
LA1	OPy	1,002	4,318	58	37	1,268	319	bdl	bdl	bdl	bdl	bdl	bdl	21	bdl	bdl	379,757
LA2	OPy	1,453	9,879	bdl	14	1,026	142	6	21	bdl	99	75	bdl	25	bdl	bdl	510,778
LA3	PrePy2	bdl	53	bdl	2	bdl	8	bdl	bdl	bdl	bdl	137	93	27	bdl	bdl	380,578
LA4	PrePy2	bdl	bdl	bdl	bdl	bdl	bdl	bdl	25	bdl	bdl	bdl	bdl	11	310	bdl	373,094
Figure 6A (SYD-3A-1, 32 g/t, Shuiyindong deposit)																	
LA1	OPy	986	8,090	bdl	41	2,719	271	bdl	29	bdl	bdl	30	bdl	106	bdl	38	433,400
LA2	OPy	856	5,342	bdl	4	1,234	22	bdl	bdl	bdl	bdl	19	9	bdl	bdl	bdl	329,030
LA3	OPy	837	6,289	bdl	27	2,993	254	bdl	bdl	bdl	bdl	22	70	bdl	bdl	bdl	440,488
LA4	OPy	612	9,851	bdl	7	2,621	74	bdl	bdl	bdl	98	bdl	25	25	bdl	bdl	369,403
LA5	PrePy2	bdl	1,205	bdl	bdl	bdl	bdl	bdl	bdl	bdl	bdl	88	161	bdl	bdl	bdl	253,812
LA6	PrePy2	bdl	910	bdl	bdl	125	bdl	bdl	bdl	bdl	59	59	293	5	bdl	bdl	448,843
LA7	PrePy2	bdl	426	bdl	bdl	bdl	bdl	bdl	bdl	bdl	81	bdl	44	bdl	bdl	31	534,263
LA8	PrePy2	bdl	57	bdl	bdl	bdl	bdl	3	bdl	bdl	bdl	bdl	bdl	bdl	bdl	bdl	386,535

Abbreviations: bdl = below detection limit, OPy = ore pyrite, PrePy2 = pre-ore pyrite 2
[1]Value listed below the element is the approximate detection limit (in ppm)
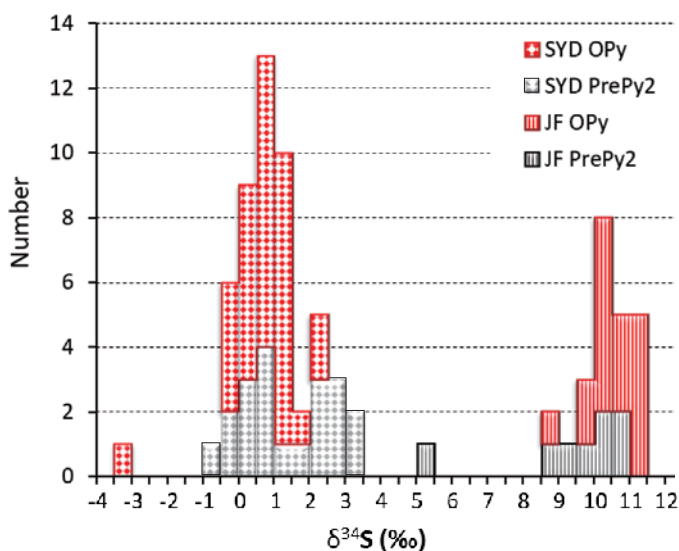
Fig. 8. Histogram of all δ^{34}S isotope data gathered in this study from pre-ore pyrite 2 (PrePy2) and ore pyrite (Opy) from the Shuiyindong (SYD) and Jinfeng (JF) deposits. See Table 5 for analysis details.

Comparison of Guizhou sediment-hosted Au deposit sulfur isotopes

Available δ^{34}S data for pre-ore and ore pyrites, ore- and late ore-stage arsenopyrite, and late ore-stage sulfide minerals including stibnite, realgar, orpiment, and cinnabar from several Guizhou sediment-hosted Au deposits (Guo, 1988; Li et al., 1989, 1995; Li, 1994; Liu et al., 1994; Zhang et al., 2003; Xia, 2005; Wang et al., 2010, 2012, 2013b; Zhang et al., 2010; Fan, 2015; Tan et al., 2015b; Hou et al., 2016; Wei, 2017; Zheng, 2017; Yan et al., 2018) are compiled for comparison (Fig. 9). Sulfur isotope data for pre-ore pyrites include both in situ and available bulk analyses because all of these data can provide a pure pre-ore S isotope signature. Sulfur isotope compositions of ore pyrite and arsenopyrite include only data obtained using in situ measurements with SHRIMP, LA-MC-ICP-MS, and nanoSIMS instruments to avoid contamination by non-ore pyrites. For the late ore-stage sulfide minerals stibnite, realgar, orpiment, and cinnabar, we include bulk analysis data as these minerals are commonly coarse and homogeneous.

Results show that pre-ore-stage pyrites from Guizhou sediment-hosted Au deposits have a broad range of δ^{34}S values

Table 5. LA-MC-ICP-MS In Situ S Isotope Compositions of Pyrites from Shuiyindong and Jinfeng Deposits

Deposit	Sample no.	Pyrite type	δ^{34}S (‰)	Deposit	Sample no.	Pyrite type	δ^{34}S (‰)
Shuiyindong	SYD-3A-1 (Au: 32 g/t)	PrePy2	−0.8	Shuiyindong	SYD-3A-1 (Au: 32 g/t)	OPy	1.0
		PrePy2	−0.5			OPy	1.0
		PrePy2	−0.3			OPy	1.1
		PrePy2	0.1			OPy	1.2
		PrePy2	0.4			OPy	1.2
		PrePy2	0.4			OPy	1.3
		PrePy2	0.5			OPy	1.3
		PrePy2	0.6			OPy	1.3
		PrePy2	0.6			OPy	1.4
		PrePy2	0.7			OPy	1.4
		PrePy2	1.3			OPy	1.5
		PrePy2	2.0			OPy	1.7
		PrePy2	2.4			OPy	2.5
		PrePy2	2.5				
		PrePy2	2.5	Jinfeng	HDDS0091-507 (Au: 28 g/t)	PrePy2	5.1
		PrePy2	2.6			PrePy2	8.9
		PrePy2	2.7			PrePy2	9.5
		PrePy2	3.0			PrePy2	9.9
		PrePy2	3.3			PrePy2	10.1
		PrePy2	3.4			PrePy2	10.2
		OPy	−3.3			PrePy2	10.5
		OPy	−0.4			PrePy2	10.5
		OPy	−0.1			OPy	8.9
		OPy	0.0			OPy	9.7
		OPy	0.0			OPy	9.8
		OPy	0.2			OPy	10.1
		OPy	0.3			OPy	10.1
		OPy	0.4			OPy	10.2
		OPy	0.5			OPy	10.3
		OPy	0.5			OPy	10.3
		OPy	0.5			OPy	10.4
		OPy	0.6			OPy	10.5
		OPy	0.6			OPy	10.6
		OPy	0.7			OPy	10.6
		OPy	0.7			OPy	11.0
		OPy	0.7			OPy	11.1
		OPy	0.7			OPy	11.1
		OPy	0.7			OPy	11.2
		OPy	0.8			OPy	11.2

Abbreviations: OPy = ore pyrite, PrePy2 = pre-ore pyrite 2

from –33.8 to +17.9‰ (Fig. 9), and in the Getang deposit the range reaches 46.7‰ (Fig. 9). Additionally, the $\delta^{34}S$ values for pre-ore-stage pyrites from different deposits are different (Fig. 9). For example, the Shuiyindong pre-ore-stage pyrites exhibit $\delta^{34}S$ values between –25.7 and +17.9‰, and most of the data plot between ~–2.1 and +3.8‰. However, the pre-ore-stage pyrites from Jinfeng deposit have $\delta^{34}S$ values ranging from 5.1 to 13.2‰, with most data between ~7.4 and 10.5‰ (Fig. 9).

Ore-related sulfide minerals including ore pyrite, arsenopyrite, and late ore-stage sulfide minerals in all deposits, except Jinfeng, have very similar $\delta^{34}S$ values, and most of these data plot between ~–5 and +5‰ (Fig. 9). The variation of $\delta^{34}S$ values for ore-related sulfide minerals in all deposits, except Jinfeng, are commonly <~ 6‰ (Fig. 9). In the Jinfeng deposit, the ore pyrite exhibits $\delta^{34}S$ values ranging from 1.9 to 18.1‰, and most of the data plot between 6.6 and 11.5‰—~7 to 12‰ greater than the $\delta^{34}S$ values of ore pyrite from other Guizhou sediment-hosted Au deposits (Fig. 9). The late ore-stage sulfide minerals from the Jinfeng deposit, including stibnite, realgar, and cinnabar, have $\delta^{34}S$ values varying from 8.4 to 13.2‰—~8 to 13‰ greater than the $\delta^{34}S$ values of late ore-stage sulfide minerals from other Guizhou sediment-hosted Au deposits (Fig. 9).
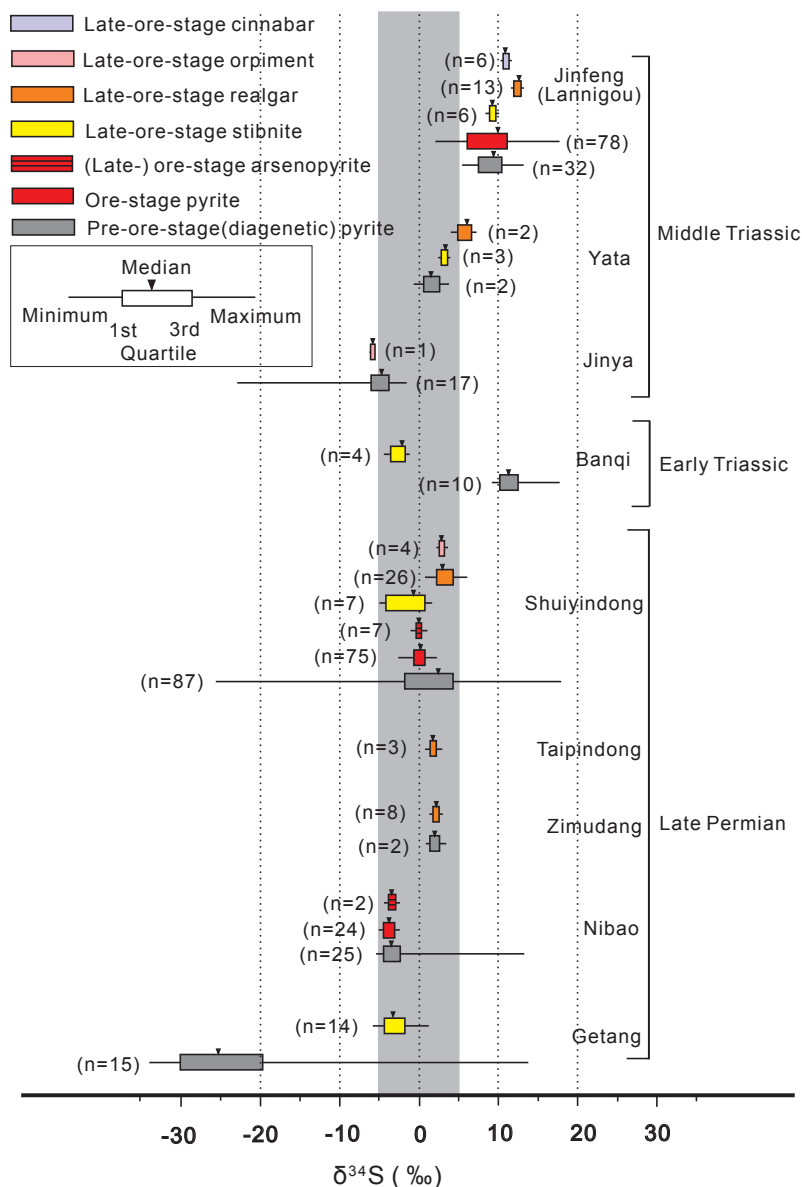
Fig. 9. Compilation of $\delta^{34}S$ isotope ratio data for pre-ore- and ore-stage pyrites from the Guizhou sediment-hosted Au deposits, including minor arsenopyrite and late ore-stage stibnite, realgar, orpiment, and cinnabar; the vertical organization of data reflects host-rock age. Pre-ore-stage pyrite types were analyzed using both bulk and in situ techniques, whereas data for ore-stage pyrite and arsenopyrite are from in situ techniques including SHRIMP, LA-MC-ICP-MS, and nanoSIMS only. Late ore-stage sulfide minerals were analyzed using bulk techniques (Guo, 1988; Li et al., 1989, 1995; Li, 1994; Liu et al., 1994; Zhang et al., 2003, 2010; Xia, 2005; Wang et al., 2010, 2012, 2013b; Fan, 2015; Tan et al., 2015b; Hou et al., 2016; Wei, 2017; Zheng, 2017; Yan et al., 2018; this study).

The broad range of S isotope compositions for the sedimentary (syngenetic or diagenetic) pyrites (pre-ore pyrites 1 and 2) is likely the result of bacterial reduction from marine sulfate during sedimentation and diagenesis in (semi-) open and sulfate-limited systems (Aharon and Fu, 2000; Machel, 2001; Shen et al., 2001; Hou et al., 2016), which is consistent with the pyrite textures (e.g., framboid and anhedral) and high concentrations of Co and low concentrations of Carlin-type elements. The narrow variation in δ^{34}S values for ore-related sulfide minerals in all Guizhou sediment-hosted Au deposits, except the Jinfeng deposit, suggests that these deposits likely formed from similarly sourced ore fluids. All Guizhou sediment-hosted Au deposits share consistently similar geologic characteristics, including ore minerals, ore fluid temperatures and pressures, and alteration minerals and textures (Su et al., 2018; Xie et al., 2018). Thus, these deposits most likely formed in response to a single widespread metallogenic event.

Jinfeng ore pyrite has a relatively broad range of S isotope compositions and is more enriched in higher δ^{34}S values than ore pyrite from other Guizhou sediment-hosted Au deposits (Fig. 9). Mixing of ore fluids with basin brines with elevated δ^{34}S value (>18‰; Yan et al., 2018) could have produced the higher values observed in this deposit. In addition, nanoSIMS analyses (Yan et al., 2018), which have a smaller beam size (1–2 μm), provided δ^{34}S values of 1.1 to 7.9‰ (most data <5‰) for As-rich bands in the ore pyrite inner rim, and values of 4.9 to 18.1‰ for the ore pyrite outer rim. These results are consistent with an interpretation that the inner ore pyrite rim precipitated from initial ore fluids with δ^{34}S values of ~1.1 to 7.9‰ that represent the S isotope signature of ore fluids, and the outer ore pyrite rim formed from ore fluids mixed with basin brines with elevated δ^{34}S value (>18‰). Owing to a larger spot size, our LA-MC-ICP-MS analyses for Jinfeng ore pyrite analyzed both inner and outer ore-stage rims, yielding δ^{34}S values between these two end-member values. Collectively, these data indicate that Jinfeng S isotope compositions of the ore pyrite inner rim (1.1–7.9‰) represent the S isotope signature of the initial ore fluids, and these values are largely consistent with the δ^{34}S values (–5–+5‰) of ore-related sulfide minerals from other Guizhou sediment-hosted Au deposits.

Source of sulfur and ore fluids

In the Carlin-type ore systems, as ore fluids were enriched in reduced S and Au was principally transported as an Au-HS complex [Au(HS)^0 and/or Au(HS)$_2^-$] (Seward, 1973, 1991; Stefánsson and Seward, 2004; William-Jones et al., 2009; Liu et al., 2014), the S isotope ratio data can provide insight into potential Au and ore fluid sources. In the Guizhou sediment-hosted Au deposits, fluid inclusion studies indicate that these deposits formed at temperatures of 190° to 300°C (average ~250°C; Zhang et al., 2003; Su et al., 2009, 2018; Wang et al., 2013a). The S isotope fractionation between pyrite and hydrothermal fluids [$\Delta(\delta^{34}S_{FeS_2}-\delta^{34}S_{HS^-})$] is less than 2‰ at a temperature of ~250°C (Ohmoto, 1972), and the $\delta^{34}S_{HS^-}$ is approximately equal to the $\delta^{34}S_{sulfide\ minerals}$ (Ohmoto and Goldhaber, 1997). Thus, the initial ore fluid should have had δ^{34}S values similar to the δ^{34}S values of sulfide minerals, between ~–5 and +5‰. Such values can result from a magmatic, metamorphic, or sedimentary S source. Because a sedimentary S

source would likely have provided a wide range of values for S in ore-stage minerals among different deposits, and because a wide range is only observed at the Jingfeng deposit, possibly owing to mixture with a fluid with elevated δ^{34}S value, we do not consider a sedimentary source as likely. Furthermore, as the sedimentary rocks that comprise the Youjiang Basin did not undergo metamorphism, a potential magmatic S source is more likely.

Known igneous rocks in the Youjiang Basin are scarce; however, minor alkaline ultramafic dikes (85–88 Ma, Liu et al., 2010) and quartz porphyry dikes (95.5–97 Ma, Chen et al., 2014; Zhu et al., 2017) have been identified ~10 to 30 km from the Au deposits (Fig. 1). Additionally, quartz porphyry dikes present at Liaotun (97–99 Ma, Zhu et al., 2017) crosscut Au orebodies (Fig. 1, Chen et al., 2014). Laser ablation-ICP-MS and SIMS U-Pb dating of inherited zircons from Liaotun, Bama, and Xiabaha quartz porphyry dikes show age clusters of 130 to 140 Ma and ca. 242 Ma (Zhu et al., 2016). These were interpreted as ages of intrusions that are not exposed in these areas. Furthermore, gravity and magnetic geophysical investigations in the Shuiyindong district are consistent with the presence of a pluton ~5 km below the surface (Liu, pers. commun., 2018). Collectively, these data indicate the presence of magmatic activity that may have contributed to formation of the Guizhou sediment-hosted Au deposits.

We suggest that the thick Devonian-Triassic passive margin sequence (6–12 km) that comprises the Youjiang Basin and weak extension following sedimentation prevented igneous activity from reaching the surface. However, buoyant ore fluids released from these intrusions could have ascended along structural conduits and precipitated Au at higher crustal levels. Because the age of Au mineralization is still controversial, it is currently not possible to relate the Au mineralization to a specific episode of magmatism. Determining an accurate age for Au mineralization continues to be an urgent research issue.

Implications and Conclusions

In the Youjiang Basin, pre-ore pyrites 1 and 2 in sedimentary rocks formed during the sedimentary (syngenetic or diagenetic) process. These pyrites have a broad range of δ^{34}S isotope compositions (–33.8–+17.9‰), and the S that formed these pyrites was probably generated by bacterial reduction from marine sulfate. Trace elements As, Ni, Pb, Cu, and Co were incorporated into these pyrites during the sedimentary process.

A thick section of sedimentary rocks in Youjiang Basin including a Devonian-Triassic passive margin sequence (6–12 km) followed by weak extension prevented igneous activity in the region from reaching the current surface, except at a few locations. Ore fluids with δ^{34}S values between ~–5 and +5‰, enriched in Au, As, Cu, Sb, Hg, and Tl and deficient in Fe, were potentially released by the deep intrusions and ascended along regional structures. Where ore fluids encountered Fe-bearing carbonate-rich host rocks under appropriate pressure-temperature conditions, ore fluids reacted with and extracted Fe from Fe-bearing dolomite and sulfidized the Fe, forming Au-bearing and trace element-rich pyrite and, ultimately, the Guizhou sediment-hosted Au deposits.

At Jinfeng, ore fluids initially precipitated Au-bearing pyrite with S isotope signatures similar to the initial ore fluids ($\delta^{34}S_{ore}$

fluid ~–5–+5‰). However, as ore pyrite continued to precipitate, ore fluids mixed with local fluids with elevated $\delta^{34}S$, possibly basin brine ($\delta^{34}S_{basin\ brine}$ >18‰; Yan et al., 2018), producing ore pyrite with elevated $\delta^{34}S$ values.

Acknowledgments

REFERENCES

Aharon, P., and Fu, B.S., 2000, Microbial sulfate reduction rates and sulfur and oxygen isotope fractionations at oil and gas seeps in deepwater Gulf of Mexico: Geochimica et Cosmochimica Acta, v. 64, p. 233–246.

Arehart, G.B., 1996, Characteristics and origin of sediment-hosted disseminated gold deposits: A review: Ore Geology Reviews, v. 11, p. 383–403.

Barker, S.L., Hickey, K.A., Cline, J.S., Dipple, G.M., Kilburn, M.R., Vaughan, J.R., and Longo, A.A., 2009, Uncloaking invisible gold: Use of nanoSIMS to evaluate gold, trace elements, and sulfur isotopes in pyrite from Carlin-type gold deposits: Economic Geology, v. 104, p. 897–904.

Bureau of Geology and Mineral Resources of Guangxi Zhuang Autonomous Region, 1985, Regional geology of Guangxi Zhuang Autonomous Region: Beijing, Geological Publishing House, p. 96. (in Chinese with English abstract).

Cai, M.H., He, L.Q., Liu, G.Q., Wu, D.C., and Huang, H.M., 2006, SHRIMP zircon U-Pb dating of the intrusive rocks in the Dachang tin-polymetallic ore field, Guangxi and their geological significance: Geological Review, v. 52, p. 409–414. (in Chinese with English abstract).

Chang, Z., Large, R.R., and Maslennikov, V., 2008, Sulfur isotopes in sediment-hosted orogenic gold deposits: Evidence for an early timing and a seawater sulfur source: Geology, v. 36, p. 971–974.

Chen, M.H., Mao, J.W., Chen, Z.Y., and Zhang, W., 2009, Mineralogy of arsenian pyrites and arsenopyrites of Carlin-type gold deposits in Yunnan-Guizhou-Guangxi "golden triangle" area, southwestern China: Mineral Deposits, v. 28, p. 539–557. (in Chinese with English abstract).

Chen, M.H., Mao, J.W., Bierlein, F.P., Norman, T., and Uttley, P.J., 2011, Structural features and metallogenesis of the Carlin-type Jinfeng (Lannigou) gold deposit, Guizhou Province, China: Ore Geology Reviews, v. 43, p. 217–234.

Chen, M.H., Zhang, Y., Meng, Y.Y., Lu, G., and Liu, S.Q., 2014, The confirmation of the upper limit of metallogenetic epoch of Liaotun gold deposit in western Guangxi, China, and its implication on chronology of Carlin-type gold deposits in Yunnan-Guizhou-Guangxi "golden triangle" area: Mineral Deposits, v. 33, p. 1–13. (in Chinese with English abstract).

Cheng, Y.B., and Mao, J.W., 2010, Age and geochemistry of granites in Gejiu area, Yunnan Province, SW China: Constraints on their petrogenesis and tectonic setting: Lithos, v. 120, p. 258–276.

Cheng, Y.B., Mao, J.W., Chen, X.L., and Li, W., 2010, LA-ICP-MS zircon U-Pb dating of the Bozhushan granite in southeastern Yunnan Province and its significance: Journal of Jilin University (Earth Science Edition), v. 40, p. 869–878. (in Chinese with English abstract).

Cline, J.S., Hofstra, A.H., Muntean, J.L., Tosdal, R.M., and Hickey, K.A., 2005, Carlin-type gold deposits in Nevada: Critical geologic characteristics and viable models: Economic Geology 100th Anniversary Volume, p. 451–484.

Cline, J.S., Muntean, J.L., Gu, X.X., and Xia, Y., 2013, A comparison of Carlin-type gold deposits: Guizhou Province, golden triangle, southwest China, and northern Nevada, USA: Earth Science Frontiers, v. 20, p. 1–18.

Eldorado Gold Corporation, 2016, Eldorado Gold mineral reserves as of December 31, 2015, available at http://www.eldoradogold.com/assets/resources-and-reserves/default.aspx.

Fan, J., 2015, Study on geochemistry and metallogenic mechanism of the Getang large-scale gold ore deposit: Ph.D. thesis, Kunming, China, Kunming University of Science and Technology, 169 p. (in Chinese with English abstract).

Gregory, D.D., Large, R.R., Halpin, J.A., Baturina, E.L., Lyons, T.W., Wu, S., Danyushevsky, L., Sack, P.J., Chappaz, A., Maslennikov, V.V., and Bull, S.W., 2015, Trace element content of sedimentary pyrite in black shales: Economic Geology, v. 110, p. 1389–1410.

Guo, Z.C., 1988, The geological features and origin of the Zimudang gold deposit in Xingren County, Guizhou Province: Geology of Guizhou, v. 5, p. 201–295. (in Chinese with English abstract).

Han, Z.J., Wang, Y.G., Feng, J.Z., Chen, T.J., Luo, X.H., and Liu, Y.H., 1999, The geology and exploration of gold deposits in southwestern Guizhou, China: Guiyang, China, Guizhou Science and Technology Press, 146 p. (in Chinese with English abstract).

Hilde, T.W.C., Uyeda, S., and Kroenke, L., 1977, Evolution of the western Pacific and its margin: Tectonophysics, v. 38, p. 145–165.

Hofstra, A.H., and Cline, J.S., 2000, Characteristics and models for Carlin-type gold deposits: Reviews in Economic Geology, v. 13, p. 163–220.

Hofstra, A.H., Leventhal, J.S., Northrop, H.R., Landis, G.P., Rye, R.O., Birak, D.J., and Dahl, A.R., 1991, Genesis of sediment-hosted disseminated gold deposits by fluid mixing and sulfidization: Chemical-reaction-path modeling of ore-depositional processes documented in the Jerritt Canyon district, Nevada: Geology, v. 19, p. 36–40.

Hou, L., Peng, H.J, Ding, J., Zhang, J.R, Zhu, S.B., Wu, S.Y., Wu, Y., and Ouyang, H.G., 2016, Textures and in situ chemical and isotopic analyses of pyrite, Huijiabao trend, Youjiang Basin, China: Implications for paragenesis and source of sulfur: Economic Geology, v. 111, p. 331–353.

Hu, R.Z., Su, W.C., Bi, X.W., Tu, G.Z., and Hofstra, A.H., 2002, Geology and geochemistry of Carlin-type gold deposits in China: Mineralium Deposita, v. 37, p. 378–392.

Hu, R.Z., Peng, J.T., Ma, D.S., Su, W.C., Shi, C.H., Bi, X.W., and Tu, G.Z., 2007, Epoch of large-scale low-temperature mineralization in southwestern Yangtze massif: Mineral Deposits, v. 26, p. 583–596. (in Chinese with English abstract).

Hu, R.Z., Fu, S.L., Huang, Y., Zhou, M.F., Fu, S.H., Zhao, C.H., Wang, Y.J., Bi, X.W., and Xiao, J.F., 2017, The giant South China Mesozoic low-temperature metallogenic domain: Reviews and a new geodynamic mode: Journal of Asian Earth Sciences, v. 137, p. 9–34.

John, B.M., Zhou, X.H., and Li, J.L., 1990, Formation and tectonic evolution of southeastern China and Taiwan: Isotopic and geochemical constraints: Tectonophysics, v. 183, p. 145–160.

Kesler, S.E., Fortuna, J., Ye, Z., Alt, J.C., Core, D.P., Zohar, P., Borhauer, J., and Chryssoulis, S.L., 2003, Evaluation of the role of sulfidation in deposition of gold, Screamer section of the Betze-Post Carlin-type deposit, Nevada: Economic Geology, v. 98, p. 1137–1157.

Kesler, S.E., Riciputi, L.C., and Ye, Z., 2005, Evidence for a magmatic origin for Carlin-type gold deposits: Isotopic composition of sulfur in the Betze-Post-Screamer deposit, Nevada, USA: Mineralium Deposita, v. 40, p. 127–136.

Krouse, H.R., and Coplen, T.B., 1997, Reporting of relative sulfur isotope-ratio data: Pure and Applied Chemistry, v. 69, p. 293–295.

Lai, C.K., Meffre, S., Crawford, A.J., Zaw, K., Xue, C.D., and Halpin, J.A., 2014, The western Ailaoshan volcanic belts and their SE Asia connection: A new tectonic model for the eastern Indochina block: Gondwana Research, v. 26, p. 52–74.

Large, R.R., Maslennikov, V.V., Robert, F., Danyushevsky, L.V., and Chang, Z., 2007, Multistage sedimentary and metamorphic origin of pyrite and gold in the giant Sukhoi Log deposit, Lena gold province, Russia: Economic Geology, v. 102, p. 1233–1267.

Large, R.R., Danyushevsky, L., Hollit, C., Maslennikov, V., Meffre, S., Gilbert, S., Bull, S., Scott, R., Emsbo, P., Thomas, H., Singh, B., and Foster, J., 2009, Gold and trace element zonation in pyrite using a laser imaging

technique: Implications for the timing of gold in orogenic and Carlin-style sediment-hosted deposits: Economic Geology, v. 104, p. 635–668.

Li, C.Y., 1994, The isotope earth chemical feature of the Gaolong Au deposit and its geology significance: Journal of Precious Metallic Geology, v. 3, p. 123–130. (in Chinese with English abstract).

Li, S.R., Wang, D.H., Liang, T., Qu, W.J., and Ying, L.J., 2008, Metallogenic epochs of the Damingshan tungsten deposit in Guangxi and its prospecting potential: Acta Geologica Sinica, v. 82, p. 873–879. (in Chinese with English abstract).

Li, W.K., Jiang, X.S., Ju, R.H., Meng, F.Y., and Zhang, S.X., 1989, The geological characteristics and metallogenesis of disseminated gold deposits in southwestern Guizhou, China, in Shenyang Institute of Geology and Mineral Resources, ed., Regional ore-forming condition of main gold deposit styles in China, v. 6, southwestern Guizhou: Beijing, China, Geological Publishing House, p. 1–86. (in Chinese).

Li, Z.Q., Chen, S.D., Wang, J.Z., Li, F.C., and Wang, G.T., 1995, Isotope geochemistry of Jinya disseminated gold deposit in western Guangxi: Mineralogy and Petrology, v. 15, p. 66–72. (in Chinese with English abstract).

Li, Z.X., and Li, X.H., 2007, Formation of the 1300-km-wide intracontinental orogen and postorogenic magmatic province in Mesozoic South China: A flat-slab subduction model: Geology, v. 35, p. 179–182.

Liu, D.S., Tan, Y.J., Wang, J.Y., Wei, L.M., and Jiang, S.F., 1994, Carlin-type gold deposit in China: Nanjing, China, Nanjing University Press, p. 1–414. (in Chinese).

Liu, J.M., and Liu, J.J., 1997, Basin fluid genetic model of sediment-hosted micro-disseminated gold deposits in the gold-triangle area between Guizhou, Guangxi and Yunan: Acta Mineralogica Sinica, v. 17, p. 448–456. (in Chinese with English abstract).

Liu, J.M., Ye, J., Liu, J.J., and Gu, X.X., 2001, Relationship between sediments-hosted micro-disseminated gold deposits and basin evolution: Case study in Youjiang Basin, South China: Mineral Deposits, v. 20, p. 367–377. (in Chinese with English abstract).

Liu, J.Z., Xia, Y., Zhang, X.C., Deng, Y.M., Su, W.C., and Tao, Y., 2008, Model of strata-bounded Carlin-type gold deposit—the Shuiyindong super large gold deposit: Gold Science and Technology, v. 16, p. 1–5. (in Chinese with English abstract).

Liu, S., Su, W.C., Hu, R.Z., Feng, C.X., Gao, S., Coulson, I.M., Wang, T., Feng, G.Y., Tao, Y., and Xia, Y., 2010, Geochronological and geochemical constraints on the petrogenesis of alkaline ultramafic dykes from southwest Guizhou Province, SW China: Lithos, v. 114, p. 253–264.

Liu, W., Etschmann, B., Testemale, D., Hazemann, J.L., Rempel, K., Müller, H., and Brugger, J., 2014, Gold transport in hydrothermal fluids: Competition among the Cl⁻, Br⁻, HS⁻, and NH$_{3(aq)}$ ligands: Chemical Geology, v. 376, p. 11–19.

Liu, Y.P., Li, Z.X., and Li, H.M., 2007, U-Pb geochronology of cassiterite and zircon from the Dulong Sn-Zn deposit: Evidence for Cretaceous large-scale granitic magmatism and mineralization events in southeastern Yunnan Province, China: Acta Petrologica Sinica, v. 23, p. 967–976. (in Chinese with English abstract).

Longerich, H.P., Jackson, S.E., and Günther, D., 1996, Laser ablation inductively coupled plasma mass spectrometric transient signal data acquisition and analyze concentration calculation: Journal of Atomic Spectrometry, v. 11, p. 899–904.

Machel, H.G., 2001, Bacterial and thermochemical sulfate reduction in diagenetic settings—old and new insights: Sedimentary Geology, v. 140, p. 143–175.

Mao, J.W., Cheng, Y.B., Chen, M.H., and Franco, P., 2013, Major types and time-space distribution of Mesozoic ore deposits in South China and their geodynamic settings: Mineralium Deposita, v. 48, p. 267–294.

Maroun, L.R.C., Cline, J.S., Simon, A., Anderson, P., and Muntean, J., 2017, High-grade gold deposition and collapse breccia formation, Cortez Hills Carlin-type gold deposit, Nevada, USA: Economic Geology, v. 112, p. 707–740.

Muntean, J.L., Cline, J.S., Simon, A.C., and Longo, A.A., 2011, Magmatic-hydrothermal origin of Nevada's Carlin-type gold deposits: Nature Geoscience, v. 4, p. 122–127.

Ohmoto, H., 1972, Systematics of sulfur and carbon isotopes in hydrothermal ore deposits: Economic Geology, v. 67, p. 551–578.

Ohmoto, H., and Goldhaber, M.B, 1997, Sulphides and carbon isotopes, in Barnes, H.L., ed., Geochemistry of hydrothermal ore deposits, 3rd edition: New York, John Wiley and Sons, Inc., p. 517–612.

Peters, S.G., Huang, J., Li, Z., and Jing, C., 2007, Sedimentary rock-hosted Au deposits of the Dian-Qian-Gui area, Guizhou, and Yunnan provinces, and Guangxi district, China: Ore Geology Reviews, v. 31, p. 170–204.

Pribil, M.J., Ridley, W.I., and Emsbo, P., 2015, Sulfate and sulfide sulfur isotopes (δ^{34}S and δ^{33}S) measured by solution and laser ablation MC-ICP-MS: An enhanced approach using external correction: Chemical Geology, v. 412, p. 99–106.

Reich, M., Kesler, S.E., Utsunomiya, S., Palenik, C.S., Chryssoulis, S.L., and Ewing, R.C., 2005, Solubility of gold in arsenian pyrite: Geochimica et Cosmochimica Acta, v. 69, p. 2781–2796.

Simon, G., Kesler, S.E., and Chryssoulis, S., 1999, Geochemistry and textures of gold-bearing arsenian pyrite, Twin Creeks, Nevada: Implications for deposition of gold in Carlin-type deposits: Economic Geology, v. 94, p. 405–421.

Seward, T.M., 1973, Thio-complexes of gold in hydrothermal ore solutions: Geochimica et Cosmochimica Acta, v. 37, p. 379–399.

——1991, The hydrothermal geochemistry of gold, in Foster, R.P., eds., Gold metallogeny and exploration: Glasgow, Blackie, p. 37–62.

Shen, Y.N., Buick, R., and Canfield, D.E., 2001, Isotopic evidence for microbial sulphate reduction in the Early Archaean era: Nature, v. 410, p. 77–81.

Stefánsson, A., and Seward, T.M., 2004, Gold(I) complexing in aqueous sulphide solutions to 500°C at 500 bar: Geochimica et Cosmochimica Acta, v. 68, p. 4121–4143.

Stenger, D.P., Kesler, S.E., Peltonen, D.R., and Tapper, C.J., 1998, Deposition of gold in Carlin-type deposits: The role of sulfidation and decarbonation at Twin Creeks, Nevada: Economic Geology, v. 93, p. 201–215.

Su, W.C., Xia, B., Zhang, H.T., Zhang, X.C., and Hu, R.Z., 2008, Visible gold in arsenian pyrite at the Shuiyindong Carlin-type gold deposit, Guizhou, China: Implications for the environment and processes of ore formation: Ore Geology Reviews, v. 33, p. 667–679.

Su, W.C., Heinrich, C.A., Pettke, T., Zhang, X.C., Hu, R.Z., and Xia, B., 2009, Sediment-hosted gold deposits in Guizhou, China: Products of wall-rock sulfidation by deep crustal fluids: Economic Geology, v. 104, p. 73–93.

Su, W.C., Zhang, H.T., Hu, R.Z., Ge, X., Xia, B., Chen, Y.Y., and Zhu, C., 2012, Mineralogy and geochemistry of gold-bearing arsenian pyrite from the Shuiyindong Carlin-type gold deposit, Guizhou, China: Implications for gold depositional processes: Mineralium Deposita, v. 47, p. 653–662.

Su, W.C., Dong, W.D., Zhang, X.C., Shen, N.P., Hu, R.Z., Hofstra, A.L., Cheng, L.Z., Xia, Y., and Yang, K.Y., 2018, Carlin-style gold deposits in the Dian-Qian-Gui "golden triangle" of southwest China: Reviews in Economic Geology, v. 20, p. 157–185.

Tan, Q.P., 2015, Tectonic geochemistry and metallogenic mechanism of the Shuiyindong Carlin-type gold deposit, Guizhou, China: Ph.D. thesis, Beijing, China, University of Chinese Academy of Sciences, 136 p. (in Chinese with English abstract).

Tan, Q.P., Xia, Y., Xie, Z.J., and Yan, J., 2015a, Migration paths and precipitation mechanisms of ore-formation fluid at the Shuiyindong Carlin-type gold deposit, Guizhou, China: Ore Geology Reviews, v. 69, p. 140–156.

Tan, Q.P., Xia, Y., Xie Z.J., Yan, J., and Wei, D.T., 2015b, S, C, O, H, and Pb isotopic studies for the Shuiyindong Carlin-type gold deposit, southwest Guizhou, China: Constraints for ore genesis: Chinese Journal of Geochemistry, v. 34, p. 529–539.

Wang, C.H., Wang, D.H., Liu, J.Z., Deng, Y.M., Liu, C.Q., Li, J.K., Chen, F.E., and Zhang, J.Z., 2010, Characteristics of isotopic geochemistry Shuiyindong super-large Carlin-type gold deposit in Guizhou: Earth Science Frontiers, v. 17, p. 396–403. (in Chinese with English abstract).

Wang, G.Z., Hu, R.Z., Su, W.C., and Zhu, L.M., 2002, Basin fluid migration and mineralization of Youjiang Basin, Dian-Qian-Gui area: Science in China (Series D), v. 32, p. 78–86. (in Chinese with English abstract).

Wang, Y.G., 1990, Two gold-bearing sequences and their sedimentary environments in southwestern Guizhou and its adjacent areas: Sedimentary Facies and Paleogeography, v. 6, p. 8–13. (in Chinese with English abstract).

Wang, Z.P., Xia, Y., Song, X.Y., You, B., Zheng, X.H., and Wang, X.Y., 2012, Isotopes and REE characteristic and ore-forming materials source of the Taipingdong-Zimudang gold deposit: Acta Mineralogica Sinica, v. 32, p. 93–100. (in Chinese with English abstract).

Wang, Z.P., Xia, Y., Song, X.Y., Liu, J.Z., Yang, C.F., and Yan, B.W., 2013a, Study on the evolution of ore-formation fluids for Au-Sb ore deposits and the mechanism of Au-Sb paragenesis and differentiation in the southwestern part of Guizhou Province, China: Chinese Journal of Geochemistry, v. 32, p. 56–68.

Wang, Z.P., Xia, Y., Song, X.Y., Yan, B.W., and Tan, Q.P., 2013b, Sulfur and lead isotope composition of the Huijiabao Carlin-type Au field and the ore forming material sources in southwest Guizhou: Bulletin of Mineralogy, Petrology and Geochemistry, v. 32, p. 746–759. (in Chinese with English abstract).

Wang, Z.S., 1997, Affirmation of the Jurassic in Longtoushan of Zhenfeng, Guizhou, and its geological significance: Guizhou Geology, v. 14, p. 201–203. (in Chinese with English abstract).

Wei, D.T., 2017, Study on the ore-forming source, the hydrothermal evolution and the ore-forming mechanism of the Nibao gold deposit, southwestern Guizhou Province, China: Ph.D. thesis, Beijing, China, University of Chinese Academy of Sciences, 152 p. (in Chinese with English abstract).

Williams-Jones, A.E., Bowell, R.J., and Migdisov, A.A., 2009, Gold in solution: Elements, v. 5, p. 281–287.

Xia, Y., 2005, Characteristics and model for Shuiyindong Au deposit in southwestern Guizhou, China: Ph.D. thesis, Guiyang, China, Institute of Geochemistry, Chinese Academy of Sciences, 123 p. (in Chinese with English abstract).

Xia, Y., Zhang, Y., Su, W.C., Tao, Y., Zhang, X.C., Liu, J.Z., and Deng, Y.M., 2009, Metallogenic model and prognosis of the Shuiyindong super large stratabound Carlin-type Au deposit, southwestern Guizhou Province, China: Acta Geologica Sinica, v. 83, p. 1473–1482. (in Chinese with English abstract).

Xie, Z.J., Xia, Y., Cline, J.S., Yan, B.W., Wang, Z.P., Tan, Q.P., and Wei, D.T., 2017, Comparison of the native antimony-bearing Paiting gold deposit, Guizhou Province, China with Carlin-type gold deposits, Nevada, USA: Mineralium Deposita, v. 52, p. 69–84.

Xie, Z.J., Xia, Y., Cline, J.S., Alan, K., Wei, D.T., Tan, Q.P., and Wang, Z.P., 2018, Are there Carlin-type Au deposits in China? A comparison between the Guizhou China and Nevada USA deposits: Reviews in Economic Geology, v. 20, p. 187–233.

Xu, B., Jiang, S.Y., Wang, R., Ma, L., Zhao, K.D., and Yan, X., 2015, Late Cretaceous granites from the giant Dulong Sn-polymetallic ore district in Yunnan Province, South China: Geochronology, geochemistry, mineral chemistry and Nd-Hf isotopic compositions: Lithos, v. 218, p. 54–72.

Yan, J., Hu, R.Z., Liu, S., Lin, Y.T., Zhang, J.C., and Fu, S.L., 2018, Nano-SIMS element mapping and sulfur isotope analysis of Au-bearing pyrite from Lannigou Carlin-type Au deposit in SW China: New insights into the origin and evolution of Au-bearing fluids: Ore Geology Reviews, v. 92, p. 29–41.

Ye, Z.J., Kesler, S.E., Essene, E.J., Zohar, P.B., and Borhauer, J.L., 2003, Relation of Carlin-type gold mineralization to lithology, structure and alteration: Screamer zone, Betze-Post deposit, Nevada: Mineralium Deposita, v. 38, p. 22–38.

Zaw, K., Meffre, S., Lai, C.K., Burrett, C., Santosh, M., Graham, I., Manaka, T., Salam A., Kamvong, T., and Cromie, P., 2014, Tectonic and metallogeny of mainland Southeast Asia: A review and contribution: Gondwana Research, v. 26, p. 5–30.

Zhang, X.C., Spiro, B., Halls, C., Stanley, C., and Yang, K.Y., 2003, Sediment-hosted disseminated gold deposits in southwest Guizhou, PRC: Their geological setting and origin in relation to mineralogical, fluid inclusion, and stable-isotope characteristics: International Geology Review, v. 45, p. 407–470.

Zhang, Y., Xia, Y., Wang, Z.P., Yan, B.W., Fu, Z.K., and Chen, M., 2010, REE and stable isotope geochemical characteristics of Bojitian Au deposit, Guizhou Province: Earth Science Frontiers, v. 17, p. 385–395. (in Chinese with English abstract).

Zheng, L.L., 2017, Mineralization mechanism and ore-forming process of the Nibao gold deposit in southwestern Guizhou, China: Ph.D. thesis, Guiyang, China, Guizhou University, 141 p. (in Chinese with English abstract).

Zhu, J.J., Zhong, H., Xie, G.Q., Zhao, C.H., Xu, L.L., and Lu, G., 2016, Origin and geological implication of the inherited zircon from felsic dykes, Youjiang Basin, Chian: Acta Petrologica Sinica, v. 32, p. 3269–3280. (in Chinese with English abstract).

Zhu, J.J., Hu, R.Z., Richards, J.P., Bi, X.W., Stern, R., and Lu, G., 2017, No genetic link between Late Cretaceous felsic dikes and Carlin-type Au deposits in the Youjiang Basin, southwest China: Ore Geology Reviews, v. 84, p. 328–337.

APPENDIX 1

Detection Limit for LA-ICP-MS Analysis

Element	LA-ICP-MS detection limit (ppm)	Element	LA-ICP-MS detection limit (ppm)
Au	1–3	Zn	130–270
As	10–470	Mo	7–40
Sb	3–8	Fe	400–700
Hg	10–50	S	18,000–70,000
Tl	2–5	V	15–70
Cu	10–35	Cr	20–140
Bi	2–4	Mn	30–55
Ag	5–15	Cd	20–45
Te	10–15	Sn	3–8
Co	10–35	Se	80–910
Ni	20–150	Pb	2–6

APPENDIX 2

Pyrite Chemistry (in ppm) Analyzed by LA-ICP-MS

Deposit	Pyrite type	Sample and Au grade	S	V	Cr	Mn	Co	Ni	Cu
Shuiyindong	PrePy1	SYD-2F-3 at 80 g/t	539,459.3	bdl	bdl	118.2	371.9	1,436.3	154.3
Shuiyindong	PrePy1	SYD-2F-3 at 80 g/t	635,883.8	bdl	bdl	bdl	1,302.4	3,066.9	77.1
Shuiyindong	PrePy1	SYD-2F-3 at 80 g/t	485,559.3	bdl	bdl	105.1	995.1	2,569.4	162.5
Shuiyindong	PrePy1	SYD-2F-3 at 80 g/t	455,496.5	bdl	bdl	82.4	391.5	736.6	95.6
Shuiyindong	PrePy1	SYD-2F-3 at 80 g/t	484,896.0	bdl	bdl	bdl	131.6	bdl	bdl
Shuiyindong	PrePy1	34332-45 at 3.56 g/t	708,907.9	bdl	bdl	59.7	616.7	113.0	155.7
Jinfeng	PrePy2	HDDS0154B-777 at 0.02 g/t	670,166.4	bdl	92.3	bdl	20.5	bdl	166.9
Jinfeng	PrePy2	HDDS0154B-777 at 0.02 g/t	503,536.7	bdl	82.7	bdl	98.3	bdl	392.6
Jinfeng	PrePy2	HDDS0154B-777 at 0.02 g/t	472,838.7	179.6	bdl	109.9	bdl	bdl	201.7
Jinfeng	PrePy2	HDDS0154B-777 at 0.02 g/t	508,208.2	bdl	bdl	bdl	bdl	165.4	340.1
Jinfeng	PrePy2	HDDS0154B-740 at 1.62 g/t	657,888.6	bdl	bdl	bdl	bdl	bdl	735.5
Jinfeng	PrePy2	HDDS0154B-740 at 1.62 g/t	447,023.0	bdl	bdl	31.7	25.3	bdl	1,956.3
Jinfeng	PrePy2	HDDS0154B-766 at 57 g/t	677,919.8	bdl	bdl	bdl	28.2	bdl	bdl
Jinfeng	PrePy2	HDDS0170-592 at 0.02 g/t	283,700.8	186.2	bdl	bdl	bdl	bdl	4,837.3
Jinfeng	PrePy2	HDDS0170-592 at 0.02 g/t	640,622.2	bdl	bdl	bdl	bdl	bdl	3,942.7
Jinfeng	PrePy2	HDDS0170-592 at 0.02 g/t	498,341.9	bdl	60.5	bdl	20.1	bdl	2,042.1
Shuiyindong	PrePy2	SYD-3A-1 at 31.9 g/t	253,812.0	bdl	bdl	bdl	87.8	161.5	bdl
Shuiyindong	PrePy2	SYD-3A-1 at 31.9 g/t	448,842.6	bdl	bdl	59.4	59.2	293.0	125.5
Shuiyindong	PrePy2	SYD-3A-1 at 31.9 g/t	534,263.4	bdl	bdl	81.3	bdl	43.7	bdl
Shuiyindong	PrePy2	SYD-3A-1 at 31.9 g/t	386,534.9	bdl	bdl	bdl	bdl	bdl	bdl
Shuiyindong	PrePy2	9-1200-3A at 40 g/t	380,577.5	bdl	bdl	bdl	137.2	92.8	bdl
Shuiyindong	PrePy2	9-1200-3A at 40 g/t	373,094.4	bdl	bdl	bdl	bdl	bdl	bdl
Shuiyindong	PrePy2	34332-45 at 3.56 g/t	595,048.3	45.2	bdl	250.7	99.3	255.2	1,418.0
Shuiyindong	PrePy2	34332-45 at 3.56 g/t	708,052.8	bdl	bdl	bdl	bdl	347.3	bdl
Shuiyindong	PrePy2	34332-45 at 3.56 g/t	504,443.4	bdl	bdl	bdl	921.3	291.2	300.3
Shuiyindong	PrePy2	34332-42 at 0.16 g/t	144,072.0	bdl	bdl	bdl	bdl	61.1	bdl
Shuiyindong	PrePy2 + PrePy3	SYD-3A-1 at 31.9 g/t	561,014.2	bdl	bdl	bdl	26.4	176.5	bdl
Shuiyindong	PrePy2 + PrePy3	SYD-3A-1 at 31.9 g/t	807,816.7	bdl	302.3	93.3	46.7	978.9	bdl
Jinfeng	PrePy3	HDDS0154B-777 at 0.02 g/t	430,015.5	bdl	bdl	bdl	bdl	bdl	78.3
Jinfeng	PrePy3	HDDS0154B-777 at 0.02 g/t	593,827.2	bdl	bdl	53.1	bdl	bdl	250.5
Jinfeng	PrePy3	HDDS0154B-777 at 0.02 g/t	681,701.9	bdl	bdl	1,213.4	7,461.2	1,259.6	230.6
Jinfeng	PrePy3	HDDS0170-592 at 0.02 g/t	474,330.6	bdl	bdl	bdl	98.8	244.0	1,377.4
Jinfeng	PrePy3	HDDS0170-592 at 0.02 g/t	438,994.2	bdl	bdl	bdl	35.5	bdl	307.0
Shuiyindong	PrePy3	34332-42 at 0.16 g/t	379,253.5	bdl	bdl	bdl	234.2	144.7	590.8
Shuiyindong	PrePy3	34332-42 at 0.16 g/t	366,079.4	bdl	82.5	bdl	185.3	98.6	628.0
Jinfeng	PrePy4	HDDS0170-592 at 0.02 g/t	504,265.1	77.2	305.4	bdl	141.4	270.9	298.8
Jinfeng	PrePy4	HDDS0170-592 at 0.02 g/t	428,010.4	bdl	bdl	59.4	bdl	bdl	bdl
Jinfeng	PrePy4	HDDS0170-592 at 0.02 g/t	727,518.5	bdl	bdl	bdl	bdl	180.9	1,189.2
Jinfeng	PrePy4	HDDS0170-592 at 0.02 g/t	653,307.7	bdl	85.4	52.3	bdl	145.9	463.9
Jinfeng	PrePy4	HDDS0170-592 at 0.02 g/t	602,101.1	bdl	bdl	43.7	bdl	bdl	2,188.5
Shuiyindong	PrePy4	34332-42 at 0.16 g/t	355,233.4	bdl	bdl	bdl	bdl	bdl	84.3
Jinfeng	Opy	HDDS0154B-740 at 1.62 g/t	742,203.8	bdl	bdl	66.7	96.8	bdl	494.7
Jinfeng	Opy	HDDS0154B-740 at 1.62 g/t	627,149.4	bdl	bdl	bdl	60.7	425.3	850.3
Jinfeng	Opy	HDDS0154B-740 at 1.62 g/t	572,040.6	23.9	bdl	bdl	bdl	bdl	195.6
Jinfeng	Opy	HDDS0154B-740 at 1.62 g/t	116,756.1	bdl	bdl	bdl	bdl	bdl	83.1
Jinfeng	Opy	HDDS0154B-766 at 57 g/t	649,279.6	bdl	bdl	90.4	bdl	191.0	188.7
Jinfeng	Opy	HDDS0154B-766 at 57 g/t	603,146.1	bdl	155.8	bdl	149.3	332.2	505.8
Jinfeng	Opy	HDDS0154B-766 at 57 g/t	669,021.6	48.2	118.6	bdl	bdl	bdl	371.8
Jinfeng	Opy	HDDS0154B-767 at 91.7 g/t	667,406.6	bdl	bdl	bdl	bdl	bdl	1,138.5
Jinfeng	Opy	HDDS0154B-767 at 91.7 g/t	332,440.9	bdl	bdl	34.9	80.6	bdl	592.3
Jinfeng	Opy	HDDS0154B-767 at 91.7 g/t	561,134.8	bdl	bdl	bdl	19.1	bdl	1,848.9
Jinfeng	Opy	HDDS0091-507 at 28.4 g/t	373,120.2	64.6	bdl	bdl	142.5	315.6	2,137.5
Jinfeng	Opy	HDDS0154B-766 at 57 g/t	325,129.6	23.3	bdl	51.5	43.6	bdl	1,686.6
Jinfeng	Opy	HDDS0154B-766 at 57 g/t	825,293.3	bdl	94.0	bdl	bdl	bdl	316.3
Jinfeng	Opy	HDDS0154B-766 at 57 g/t	624,462.0	bdl	bdl	86.4	bdl	bdl	1,498.2
Jinfeng	Opy	HDDS0154B-766 at 57 g/t	736,888.1	bdl	bdl	bdl	bdl	bdl	2,236.8
Jinfeng	Opy	HDDS0154B-766 at 57 g/t	815,233.0	bdl	bdl	106.8	bdl	bdl	370.2
Jinfeng	Opy	HDDS0154B-766 at 57 g/t	827,279.1	bdl	bdl	bdl	bdl	bdl	142.7
Jinfeng	Opy	HDDS0154B-766 at 57 g/t	732,056.2	bdl	bdl	166.2	bdl	bdl	806.1
Jinfeng	Opy	HDDS0154B-766 at 57 g/t	534,479.2	bdl	bdl	bdl	bdl	bdl	1,582.5
Jinfeng	Opy	HDDS0154B-766 at 57 g/t	722,579.6	bdl	bdl	bdl	bdl	bdl	623.5
Jinfeng	Opy	HDDS0154B-767 at 91.7 g/t	432,331.7	bdl	bdl	55.6	125.3	bdl	1,268.7
Jinfeng	Opy	HDDS0154B-767 at 91.7 g/t	570,287.3	bdl	bdl	bdl	141.1	bdl	168.4
Jinfeng	Opy	HDDS0154B-767 at 91.7 g/t	923,653.9	bdl	bdl	bdl	367.6	265.3	852.7

APPENDIX 2. *(Cont.)*

Deposit	Zn	As	Se	Mo	Ag	Cd	Sn	Sb	Au	Hg	Tl	Pb	Bi
Shuiyindong	bdl	1,357.5	bdl	42.4	bdl	bdl	bdl	151.5	bdl	42.9	9.2	121.7	bdl
Shuiyindong	bdl	928.5	bdl	41.6	18.3	9.7	bdl	260.0	bdl	68.9	38.8	173.2	5.7
Shuiyindong	bdl	1,174.3	bdl	bdl	bdl	bdl	bdl	197.8	bdl	4.4	30.6	164.6	bdl
Shuiyindong	bdl	712.9	bdl	bdl	9.4	18.6	bdl	179.6	bdl	51.8	14.9	74.8	bdl
Shuiyindong	265.4	64.0	bdl	bdl	13.5	bdl	bdl	94.5	bdl	55.8	31.7	49.5	bdl
Shuiyindong	bdl	3,463.0	bdl	bdl	bdl	bdl	bdl	116.7	bdl	147.6	63.0	101.4	bdl
Jinfeng	bdl	11,678.9	bdl	bdl	12.7	bdl	39.7	41.9	bdl	bdl	bdl	28.9	bdl
Jinfeng	278.3	365.6	bdl	bdl	bdl	bdl	46.5	316.4	bdl	bdl	bdl	369.1	4.2
Jinfeng	bdl	1,637.1	bdl	bdl	12.8	567.6	bdl	55.9	bdl	bdl	bdl	42.3	bdl
Jinfeng	bdl	652.6	bdl	bdl	bdl	bdl	bdl	532.6	4.0	bdl	bdl	456.7	12.4
Jinfeng	549.8	2,575.4	bdl	bdl	bdl	bdl	bdl	194.7	2.3	12.4	bdl	1,344.4	bdl
Jinfeng	bdl	1,239.6	bdl	bdl	7.6	bdl	47.0	324.8	bdl	11.2	4.0	883.7	14.7
Jinfeng	bdl	2,397.8	bdl	bdl	bdl	142.9	bdl	46.8	bdl	13.3	bdl	67.1	bdl
Jinfeng	bdl	348.4	bdl	bdl	bdl	bdl	65.3	424.0	bdl	72.9	bdl	1,072.0	9.6
Jinfeng	bdl	540.7	bdl	bdl	bdl	bdl	25.2	163.6	bdl	bdl	bdl	351.5	9.6
Jinfeng	bdl	1,127.2	1,010.3	8.2	bdl	bdl	26.5	170.7	bdl	bdl	bdl	697.6	15.8
Shuiyindong	bdl	1,204.8	177.3	bdl	bdl	bdl	bdl	bdl	bdl	bdl	bdl	bdl	bdl
Shuiyindong	bdl	909.5	bdl	bdl	bdl	bdl	bdl	bdl	bdl	bdl	bdl	4.6	bdl
Shuiyindong	bdl	425.7	bdl	bdl	bdl	bdl	31.2	bdl	bdl	bdl	bdl	bdl	bdl
Shuiyindong	bdl	57.3	bdl	bdl	bdl	bdl	bdl	bdl	bdl	bdl	bdl	bdl	3.2
Shuiyindong	bdl	53.0	bdl	bdl	bdl	bdl	bdl	8.2	bdl	bdl	2.1	27.3	bdl
Shuiyindong	310.2	64.0	164.0	bdl	25.3	bdl	bdl	bdl	4.7	bdl	bdl	11.1	bdl
Shuiyindong	bdl	7,076.9	9,757.0	bdl	15.7	bdl	186.8	460.1	bdl	bdl	17.3	411.6	bdl
Shuiyindong	bdl	64.0	bdl	11.6	bdl	bdl	bdl	12.6	bdl	bdl	bdl	19.2	bdl
Shuiyindong	bdl	556.6	bdl	bdl	7.7	bdl	bdl	bdl	bdl	bdl	bdl	24.4	bdl
Shuiyindong	296.5	4,518.7	bdl	bdl	bdl	bdl	bdl	bdl	bdl	22.7	bdl	6.1	bdl
Shuiyindong	bdl	8,605.1	bdl	bdl	bdl	bdl	bdl	25.3	bdl	bdl	3.6	12.5	7.4
Shuiyindong	bdl	11,950.5	bdl	bdl	bdl	12.9	bdl	bdl	bdl	bdl	bdl	32.2	bdl
Jinfeng	562.1	7,758.6	bdl	bdl	bdl	168.7	bdl	36.8	bdl	bdl	bdl	43.2	bdl
Jinfeng	bdl	19,774.3	bdl	18.9	bdl	124.9	bdl	29.4	3.8	12.5	2.9	27.7	bdl
Jinfeng	635.7	13,764.1	bdl	281.9	14.3	108.8	bdl	636.4	8.8	117.5	15.7	971.3	114.3
Jinfeng	bdl	9,550.7	bdl	bdl	bdl	bdl	bdl	bdl	bdl	bdl	3.3	17.2	bdl
Jinfeng	192.6	4,278.5	1,000.7	bdl	bdl	bdl	bdl	20.4	bdl	bdl	bdl	33.6	bdl
Shuiyindong	bdl	11,630.7	bdl	bdl	bdl	bdl	bdl	bdl	bdl	bdl	bdl	18.6	bdl
Shuiyindong	bdl	30,176.3	bdl	bdl	32.3	bdl	bdl	158.5	bdl	bdl	bdl	81.2	27.0
Jinfeng	1,184.7	2,612.6	bdl	bdl	bdl	bdl	bdl	280.8	bdl	bdl	6.8	285.7	6.6
Jinfeng	bdl	604.4	bdl	bdl	bdl	bdl	bdl	39.9	bdl	bdl	2.0	17.2	bdl
Jinfeng	bdl	2,864.4	bdl	bdl	9.4	1,265.6	bdl	89.3	3.3	57.6	6.0	209.5	2.6
Jinfeng	bdl	2,055.0	bdl	bdl	42.6	bdl	bdl	156.5	bdl	bdl	11.8	237.9	2.8
Jinfeng	348.5	917.7	bdl	10.2	bdl	494.4	bdl	226.9	bdl	bdl	3.5	311.3	2.9
Shuiyindong	bdl	3,002.8	bdl	bdl	bdl	bdl	bdl	7.7	3.5	bdl	bdl	bdl	bdl
Jinfeng	540.8	23,810.9	bdl	16.4	bdl	bdl	bdl	61.9	82.3	41.9	bdl	42.9	6.3
Jinfeng	bdl	9,654.7	bdl	bdl	bdl	216.2	bdl	85.5	244.6	bdl	bdl	35.3	bdl
Jinfeng	bdl	18,358.5	bdl	bdl	bdl	bdl	bdl	16.0	47.7	bdl	bdl	124.9	bdl
Jinfeng	bdl	2,589.5	bdl	bdl	bdl	bdl	bdl	bdl	16.9	bdl	bdl	bdl	bdl
Jinfeng	bdl	32,229.3	bdl	bdl	bdl	bdl	bdl	14.4	7.0	bdl	3.9	bdl	bdl
Jinfeng	bdl	16,735.4	bdl	bdl	bdl	bdl	bdl	270.8	65.7	46.4	16.2	219.8	5.4
Jinfeng	247.1	23,904.0	bdl	bdl	9.5	bdl	bdl	197.0	3.3	17.7	5.1	234.4	bdl
Jinfeng	bdl	18,632.0	bdl	bdl	25.9	bdl	bdl	1,306.8	2,714.1	285.2	142.5	500.5	bdl
Jinfeng	bdl	8,951.2	bdl	bdl	bdl	bdl	bdl	192.2	688.9	109.4	42.0	116.6	3.7
Jinfeng	bdl	13,693.9	bdl	24.3	12.3	bdl	73.9	345.0	1,015.6	62.7	37.0	185.0	bdl
Jinfeng	bdl	5,385.0	454.6	bdl	bdl	bdl	bdl	308.4	50.7	64.8	16.2	282.4	15.5
Jinfeng	bdl	9,499.4	bdl	bdl	326.9	bdl	bdl	32.0	518.8	25.5	11.1	49.8	bdl
Jinfeng	bdl	16,757.7	bdl	bdl	bdl	bdl	bdl	138.5	2,111.6	bdl	5.6	44.3	bdl
Jinfeng	bdl	15,050.7	bdl	bdl	10.0	153.4	bdl	71.9	1,600.2	bdl	9.7	32.6	5.9
Jinfeng	bdl	16,479.2	bdl	bdl	bdl	bdl	bdl	256.4	788.6	44.2	17.9	125.1	8.5
Jinfeng	bdl	20,775.9	bdl	bdl	bdl	bdl	bdl	201.0	2,419.7	59.0	4.0	95.5	bdl
Jinfeng	bdl	7,327.2	bdl	32.1	40.1	372.1	bdl	35.0	1,434.1	bdl	5.3	4.8	3.2
Jinfeng	1,106.3	25,668.0	116.0	65.8	14.9	268.5	bdl	400.9	3,481.2	95.0	15.0	212.6	3.6
Jinfeng	204.0	13,153.1	bdl	bdl	bdl	bdl	bdl	205.9	598.7	52.7	14.6	130.3	11.1
Jinfeng	bdl	11,454.2	bdl	bdl	8.3	bdl	bdl	52.3	2,015.1	bdl	2.5	23.6	2.8
Jinfeng	1,106.1	10,443.7	bdl	bdl	bdl	bdl	bdl	378.3	1,372.4	30.3	51.7	204.9	bdl
Jinfeng	bdl	19,517.1	bdl	bdl	26.5	bdl	bdl	756.2	992.6	582.0	19.7	285.3	bdl
Jinfeng	484.8	28,976.3	bdl	bdl	8.0	898.6	bdl	986.0	3,618.0	224.5	326.8	427.3	9.6

APPENDIX 2. *(Cont.)*

Deposit	Pyrite type	Sample and Au grade	S	V	Cr	Mn	Co	Ni	Cu
Jinfeng	Opy	HDDS0154B-767 at 91.7 g/t	737,311.1	bdl	110.9	69.5	bdl	bdl	728.9
Jinfeng	Opy	HDDS0154B-767 at 91.7 g/t	589,113.9	bdl	bdl	bdl	52.3	bdl	349.4
Jinfeng	Opy	HDDS0154B-767 at 91.7 g/t	883,152.3	70.0	321.0	bdl	24.8	bdl	930.4
Jinfeng	Opy	HDDS0154B-767 at 91.7 g/t	675,422.4	bdl	bdl	bdl	64.3	209.1	343.1
Jinfeng	Opy	HDDS0154B-767 at 91.7 g/t	414,016.6	bdl	99.3	60.7	33.2	bdl	385.8
Jinfeng	Opy	HDDS0091-507 at 28.4 g/t	417,897.5	bdl	bdl	87.7	bdl	bdl	3,098.1
Jinfeng	Opy	HDDS0091-507 at 28.4 g/t	395,682.9	bdl	162.8	bdl	bdl	82.9	3,905.4
Jinfeng	Opy	HDDS0091-507 at 28.4 g/t	361,330.3	bdl	bdl	bdl	26.3	165.3	5,190.2
Jinfeng	Opy	HDDS0091-507 at 28.4 g/t	409,594.0	bdl	139.9	bdl	25.2	bdl	2,743.2
Jinfeng	Opy	HDDS0091-507 at 28.4 g/t	430,240.4	bdl	192.9	bdl	108.5	133.8	4,241.1
Shuiyindong	Opy	SYD-3A-1 at 31.9 g/t	566,406.7	bdl	bdl	bdl	107.3	1,245.6	347.3
Shuiyindong	Opy	SYD-3A-1 at 31.9 g/t	369,402.8	bdl	167.8	98.2	bdl	25.5	2,620.7
Shuiyindong	Opy	SYD-3A-1 at 31.9 g/t	497,276.1	bdl	bdl	bdl	99.8	234.5	3,366.3
Shuiyindong	Opy	SYD-3A-1 at 31.9 g/t	330,871.0	bdl	bdl	bdl	488.3	35.4	3,171.7
Shuiyindong	Opy	9-1200-3A at 40 g/t	57,463.5	bdl	bdl	bdl	150.3	bdl	756.1
Shuiyindong	Opy	9-1200-3A at 40 g/t	510,777.7	bdl	bdl	98.5	74.5	bdl	1,026.1
Shuiyindong	Opy	34332-45 at 3.56 g/t	737,833.3	bdl	42.6	bdl	34.0	bdl	586.7
Shuiyindong	Opy	34332-45 at 3.56 g/t	1,076,201.6	bdl	bdl	bdl	bdl	bdl	787.5
Shuiyindong	Opy	34332-45 at 3.56 g/t	639,180.9	bdl	bdl	bdl	995.0	594.0	372.8
Shuiyindong	Opy	34332-45 at 3.56 g/t	809,849.9	bdl	bdl	bdl	177.2	454.6	860.4
Shuiyindong	Opy	34332-45 at 3.56 g/t	658,235.7	bdl	57.8	bdl	4,145.0	602.3	315.2
Shuiyindong	Opy	34332-45 at 3.56 g/t	623,334.2	bdl	bdl	bdl	350.6	233.0	572.7
Shuiyindong	Opy	34332-45 at 3.56 g/t	459,235.2	bdl	bdl	37.0	bdl	191.8	934.8
Shuiyindong	Opy	34332-44 at 33.38 g/t	463,550.8	bdl	143.5	bdl	74.3	65.2	2,422.3
Shuiyindong	Opy	34332-44 at 33.38 g/t	351,842.0	55.3	228.0	bdl	43.8	bdl	2,716.8
Shuiyindong	Opy	SYD-2F-3 at 80 g/t	440,140.4	bdl	bdl	bdl	70.3	174.2	104.6
Shuiyindong	Opy	SYD-2F-3 at 80 g/t	404,696.9	bdl	bdl	bdl	bdl	bdl	183.7
Shuiyindong	Opy	SYD-2F-3 at 80 g/t	585,969.7	bdl	bdl	bdl	120.1	125.9	83.8
Shuiyindong	Opy	SYD-2F-3 at 80 g/t	615,301.7	bdl	bdl	65.8	bdl	175.1	341.6
Shuiyindong	Opy	SYD-2F-3 at 80 g/t	692,245.8	bdl	bdl	bdl	73.2	795.3	58.3
Shuiyindong	Opy	SYD-2F-3 at 80 g/t	661,680.1	bdl	bdl	bdl	bdl	189.7	205.2
Shuiyindong	Opy	SYD-2F-3 at 80 g/t	562,283.3	bdl	bdl	154.6	36.6	144.1	187.1
Shuiyindong	Opy	SYD-2F-3 at 80 g/t	815,633.0	bdl	bdl	bdl	bdl	bdl	194.4
Shuiyindong	Opy	SYD-2F-3 at 80 g/t	554,727.6	bdl	bdl	bdl	21.4	204.0	216.1
Shuiyindong	Opy	SYD-2F-4 at 77.2 g/t	621,666.5	95.9	bdl	bdl	47.9	bdl	356.9
Shuiyindong	Opy	SYD-2F-4 at 77.2 g/t	757,534.9	bdl	109.0	76.1	bdl	237.4	374.0
Shuiyindong	Opy	SYD-2F-4 at 77.2 g/t	698,739.9	bdl	bdl	bdl	22.7	1,904.0	86.7
Shuiyindong	Opy	SYD-2F-4 at 77.2 g/t	483,230.1	bdl	bdl	68.7	bdl	bdl	192.1
Shuiyindong	Opy	SYD-2F-4 at 77.2 g/t	934,731.9	bdl	311.4	bdl	133.9	804.7	bdl
Shuiyindong	Opy	SYD-3A-1 at 31.9 g/t	556,343.8	bdl	bdl	bdl	bdl	168.1	516.3
Shuiyindong	Opy	SYD-3A-1 at 31.9 g/t	421,184.2	bdl	bdl	bdl	70.5	bdl	1,954.8
Shuiyindong	Opy	SYD-3A-1 at 31.9 g/t	440,851.9	bdl	bdl	bdl	26.9	21.9	1,377.0
Shuiyindong	Opy	SYD-3A-1 at 31.9 g/t	433,399.7	bdl	bdl	bdl	30.1	bdl	2,719.4
Shuiyindong	Opy	SYD-3A-1 at 31.9 g/t	329,029.8	bdl	bdl	bdl	bdl	19.1	1,233.6
Shuiyindong	Opy	SYD-3A-1 at 31.9 g/t	440,487.6	bdl	bdl	bdl	bdl	21.9	2,992.6
Shuiyindong	Opy	SYD-3A-1 at 31.9 g/t	374,109.7	bdl	bdl	bdl	290.4	360.1	2,648.1
Shuiyindong	Opy	SYD-3A-1 at 31.9 g/t	504,455.6	bdl	bdl	75.6	69.5	160.8	2,264.6
Shuiyindong	Opy	SYD-3A-1 at 31.9 g/t	484,440.6	bdl	bdl	72.5	340.5	713.6	2,844.5
Shuiyindong	Opy	SYD-3A-1 at 31.9 g/t	442,032.4	67.2	bdl	bdl	bdl	27.0	3,968.3
Shuiyindong	Opy	9-1200-3A at 40 g/t	371,056.0	bdl	bdl	bdl	63.0	62.3	851.5
Shuiyindong	Opy	9-1200-3A at 40 g/t	356,692.9	bdl	bdl	bdl	29.5	24.6	973.1
Shuiyindong	Opy	9-1200-3A at 40 g/t	374,054.9	bdl	255.6	bdl	51.3	30.5	1,139.6
Shuiyindong	Opy	9-1200-3A at 40 g/t	496,678.3	bdl	bdl	bdl	57.5	77.5	1,330.0
Shuiyindong	Opy	9-1200-3A at 40 g/t	379,756.7	bdl	bdl	bdl	bdl	bdl	1,267.5
Shuiyindong	Opy	9-1200-3A at 40 g/t	493,083.9	117.1	153.4	bdl	33.8	27.0	555.1
Shuiyindong	Opy	9-1200-3A at 40 g/t	394,167.7	bdl	bdl	114.9	214.8	181.8	1,185.8
Shuiyindong	Opy	34332-45 at 3.56 g/t	573,386.5	bdl	bdl	bdl	bdl	bdl	1,040.2
Shuiyindong	Opy	34332-45 at 3.56 g/t	647,475.2	bdl	110.9	81.1	bdl	bdl	1,723.4
Shuiyindong	Opy + PrePy1	SYD-2F-3 at 80 g/t	637,717.4	bdl	bdl	bdl	57.1	bdl	162.9
Shuiyindong	Opy + PrePy1	SYD-2F-3 at 80 g/t	634,875.4	bdl	bdl	bdl	128.4	bdl	244.4
Shuiyindong	Opy + PrePy1	SYD-2F-3 at 80 g/t	421,450.2	bdl	bdl	57.7	41.1	182.6	156.9
Shuiyindong	Opy + PrePy1	SYD-2F-3 at 80 g/t	451,618.2	bdl	bdl	bdl	88.8	253.9	35.3
Shuiyindong	Opy + PrePy1	SYD-2F-3 at 80 g/t	529,211.3	bdl	167.9	bdl	131.7	216.4	43.8
Shuiyindong	Opy + PrePy1	SYD-2F-4 at 77.2 g/t	596,733.3	72.5	bdl	144.3	142.0	775.4	bdl
Shuiyindong	Opy + PrePy1	9-1200-3A at 40 g/t	180,563.3	bdl	bdl	81.0	419.3	190.4	841.4
Shuiyindong	Opy + PrePy1	9-1200-3A at 40 g/t	393,576.8	89.4	bdl	988.1	250.5	30.4	652.8
Shuiyindong	Opy + PrePy1	9-1200-3A at 40 g/t	510,195.7	88.2	bdl	bdl	229.4	bdl	381.8
Shuiyindong	Opy + PrePy1	9-1200-3A at 40 g/t	356,558.9	bdl	374.3	521.3	37.6	bdl	1,143.8

APPENDIX 2. *(Cont.)*

Deposit	Zn	As	Se	Mo	Ag	Cd	Sn	Sb	Au	Hg	Tl	Pb	Bi
Jinfeng	489.4	7,130.6	bdl	26.1	bdl	bdl	bdl	107.9	604.7	50.2	bdl	36.4	bdl
Jinfeng	bdl	12,198.0	bdl	bdl	bdl	324.6	bdl	457.2	838.9	149.2	88.9	430.3	bdl
Jinfeng	bdl	20,381.6	bdl	bdl	bdl	158.6	bdl	711.7	2,393.3	102.9	52.4	272.5	bdl
Jinfeng	265.8	22,702.4	bdl	bdl	bdl	bdl	77.2	1,007.5	1,434.8	78.5	47.6	550.8	bdl
Jinfeng	bdl	10,893.1	bdl	bdl	13.7	bdl	bdl	335.2	1,299.5	147.8	47.3	160.9	5.6
Jinfeng	301.2	3,630.6	bdl	bdl	11.3	bdl	bdl	18.0	327.4	bdl	4.3	9.9	bdl
Jinfeng	bdl	3,269.7	bdl	bdl	bdl	bdl	30.4	75.6	510.7	bdl	bdl	12.9	bdl
Jinfeng	bdl	5,539.1	164.6	bdl	bdl	bdl	bdl	87.0	509.8	bdl	12.6	29.3	bdl
Jinfeng	542.6	5,250.7	bdl	bdl	13.0	361.7	bdl	13.6	698.7	bdl	bdl	3.9	3.9
Jinfeng	bdl	5,363.9	bdl	bdl	bdl	bdl	bdl	54.0	720.6	bdl	7.1	10.3	bdl
Shuiyindong	bdl	14,526.8	bdl	bdl	bdl	35.9	bdl	79.7	66.2	18.7	bdl	23.2	bdl
Shuiyindong	bdl	9,850.6	bdl	bdl	bdl	bdl	bdl	74.0	612.5	bdl	6.5	24.9	bdl
Shuiyindong	bdl	10,441.3	326.4	bdl	13.7	bdl	bdl	92.8	577.3	bdl	9.9	31.6	bdl
Shuiyindong	bdl	11,708.0	bdl	bdl	18.8	bdl	bdl	457.9	1,478.6	80.3	41.3	124.2	bdl
Shuiyindong	bdl	2,990.1	bdl	bdl	14.9	bdl	bdl	21.4	566.3	bdl	41.0	12.4	bdl
Shuiyindong	bdl	9,879.2	bdl	bdl	21.5	bdl	bdl	142.3	1,453.3	bdl	14.1	25.4	6.5
Shuiyindong	bdl	5,413.2	2,295.4	bdl	8.5	905.9	bdl	28.4	30.7	47.7	5.6	3.9	bdl
Shuiyindong	bdl	6,536.1	bdl	19.8	12.0	bdl	27.7	129.4	5.9	bdl	bdl	200.6	bdl
Shuiyindong	bdl	66.0	bdl	bdl	bdl	bdl	bdl	11.6	7.3	bdl	bdl	12.7	bdl
Shuiyindong	656.5	8,763.6	bdl	bdl	bdl	1,192.2	22.3	50.6	43.4	bdl	12.1	71.7	bdl
Shuiyindong	169.2	452.6	bdl	bdl	13.7	1,828.3	bdl	146.0	10.2	50.3	32.0	427.9	bdl
Shuiyindong	bdl	4,045.9	bdl	bdl	7.6	bdl	42.6	57.3	37.1	59.4	6.3	75.3	7.2
Shuiyindong	bdl	6,168.7	bdl	bdl	13.8	2,069.3	bdl	41.1	88.9	bdl	bdl	21.5	2.7
Shuiyindong	bdl	21,077.6	bdl	bdl	bdl	bdl	29.9	362.2	1,216.4	45.4	84.6	86.8	bdl
Shuiyindong	bdl	20,478.2	bdl	bdl	bdl	bdl	bdl	220.7	1,037.5	24.8	62.6	99.0	bdl
Shuiyindong	238.8	3,195.0	bdl	bdl	bdl	bdl	bdl	37.5	31.3	17.1	3.7	23.9	bdl
Shuiyindong	bdl	5,953.0	bdl	bdl	bdl	bdl	bdl	13.5	90.7	bdl	bdl	19.5	bdl
Shuiyindong	bdl	4,111.9	bdl	bdl	bdl	bdl	bdl	75.2	47.6	bdl	5.2	64.6	bdl
Shuiyindong	bdl	4,614.9	bdl	bdl	bdl	25.7	bdl	93.9	226.6	39.4	8.7	24.0	bdl
Shuiyindong	bdl	3,589.6	bdl	bdl	bdl	24.0	68.6	57.5	15.8	bdl	3.4	71.4	bdl
Shuiyindong	bdl	4,341.5	bdl	bdl	bdl	15.0	bdl	67.1	67.0	21.2	bdl	9.6	bdl
Shuiyindong	477.6	4,476.1	bdl	bdl	bdl	bdl	bdl	37.6	83.7	19.4	bdl	15.0	5.8
Shuiyindong	bdl	6,796.4	bdl	bdl	bdl	15.1	bdl	72.1	101.4	bdl	6.9	8.5	bdl
Shuiyindong	bdl	3,297.2	bdl	bdl	10.8	15.7	bdl	56.8	55.6	bdl	bdl	20.7	bdl
Shuiyindong	291.1	13,576.6	bdl	bdl	bdl	bdl	bdl	170.5	861.6	bdl	6.9	40.5	bdl
Shuiyindong	642.2	13,487.5	bdl	bdl	bdl	bdl	bdl	142.3	439.0	33.1	3.3	45.3	10.6
Shuiyindong	281.1	9,619.1	bdl	bdl	bdl	bdl	bdl	14.4	18.0	bdl	bdl	31.1	bdl
Shuiyindong	259.3	8,691.6	bdl	bdl	bdl	20.8	bdl	45.6	467.4	bdl	5.6	25.9	bdl
Shuiyindong	bdl	12,670.0	bdl	bdl	48.0	bdl	53.5	102.3	104.0	bdl	19.5	46.0	11.2
Shuiyindong	bdl	13,526.7	bdl	bdl	bdl	bdl	bdl	269.5	981.0	bdl	19.8	109.4	bdl
Shuiyindong	bdl	9,812.9	bdl	bdl	23.7	bdl	bdl	190.3	1,254.7	bdl	17.0	52.5	4.2
Shuiyindong	bdl	5,609.7	184.9	bdl	13.8	bdl	bdl	140.9	899.2	bdl	24.2	53.2	3.2
Shuiyindong	bdl	8,090.0	bdl	bdl	28.6	bdl	37.7	270.6	985.8	bdl	41.4	106.3	bdl
Shuiyindong	bdl	5,342.1	bdl	bdl	bdl	bdl	bdl	21.7	856.5	bdl	4.0	9.0	bdl
Shuiyindong	bdl	6,289.1	180.9	bdl	bdl	bdl	bdl	254.2	837.1	bdl	27.4	70.5	bdl
Shuiyindong	bdl	9,851.2	bdl	bdl	16.3	bdl	bdl	254.8	1,399.1	bdl	25.0	54.0	bdl
Shuiyindong	bdl	10,181.3	160.8	bdl	14.4	bdl	bdl	281.9	1,368.8	bdl	31.0	68.8	7.3
Shuiyindong	bdl	7,684.2	bdl	bdl	42.0	bdl	bdl	424.9	1,278.0	bdl	44.6	81.8	bdl
Shuiyindong	393.8	12,031.6	bdl	bdl	bdl	298.3	bdl	123.7	1,074.8	bdl	11.7	27.0	bdl
Shuiyindong	bdl	3,367.5	179.6	bdl	bdl	bdl	bdl	100.9	745.6	bdl	17.5	23.4	bdl
Shuiyindong	bdl	5,685.0	380.6	bdl	bdl	bdl	bdl	217.8	740.2	bdl	31.9	41.9	bdl
Shuiyindong	387.1	6,101.9	bdl	bdl	bdl	267.8	bdl	245.0	1,013.5	bdl	30.2	33.7	3.8
Shuiyindong	bdl	7,417.5	bdl	bdl	15.5	bdl	bdl	326.8	1,496.5	bdl	41.2	48.5	bdl
Shuiyindong	bdl	4,318.2	178.4	bdl	bdl	bdl	bdl	318.7	1,002.0	57.7	37.1	21.2	bdl
Shuiyindong	bdl	7,841.1	bdl	bdl	bdl	bdl	bdl	225.6	1,282.6	63.4	23.2	23.1	bdl
Shuiyindong	bdl	5,150.6	bdl	bdl	bdl	bdl	35.4	158.8	1,113.1	55.4	34.9	27.5	bdl
Shuiyindong	bdl	3,953.8	bdl	18.2	bdl	bdl	47.6	29.9	60.9	bdl	2.6	16.8	bdl
Shuiyindong	bdl	4,451.8	bdl	21.8	bdl	bdl	bdl	49.6	137.7	bdl	4.4	32.8	bdl
Shuiyindong	bdl	8,895.1	bdl	bdl	bdl	bdl	bdl	74.3	78.5	bdl	3.3	23.6	bdl
Shuiyindong	bdl	5,018.8	bdl	56.5	bdl	bdl	bdl	89.8	84.4	bdl	16.5	54.1	bdl
Shuiyindong	282.2	2,816.9	bdl	bdl	bdl	bdl	bdl	28.6	49.1	bdl	8.5	12.4	bdl
Shuiyindong	bdl	953.0	bdl	bdl	bdl	bdl	bdl	97.5	8.2	46.3	26.4	48.1	bdl
Shuiyindong	368.6	2,729.2	bdl	bdl	bdl	bdl	bdl	125.8	7.7	22.8	49.8	70.5	bdl
Shuiyindong	bdl	1,877.2	bdl	bdl	22.9	bdl	bdl	82.0	28.6	38.0	14.8	12.4	bdl
Shuiyindong	bdl	2,359.1	bdl	bdl	25.9	bdl	44.5	79.7	370.3	78.1	76.6	36.9	bdl
Shuiyindong	bdl	2,764.5	bdl	52.9	bdl	bdl	bdl	134.4	451.9	bdl	6.3	17.9	bdl
Shuiyindong	bdl	5,689.8	283.9	bdl	bdl	bdl	51.7	159.5	747.1	bdl	23.8	35.2	bdl
Shuiyindong	bdl	4,912.6	bdl	bdl	bdl	bdl	bdl	175.3	927.0	bdl	25.2	35.2	bdl

APPENDIX 2. *(Cont.)*

Deposit	Pyrite type	Sample and Au grade	S	V	Cr	Mn	Co	Ni	Cu
Shuiyindong	Opy + PrePy1	34332-44 at 33.28 g/t	347,742.0	bdl	bdl	bdl	248.6	225.1	337.2
Shuiyindong	Opy + PrePy1	34332-44 at 33.28 g/t	321,687.1	bdl	bdl	bdl	378.2	191.1	237.1
Shuiyindong	Opy + PrePy1	34332-44 at 33.28 g/t	336,612.5	bdl	121.3	228.0	190.7	bdl	892.5
Shuiyindong	Opy + PrePy1	34332-44 at 33.28 g/t	386,842.4	bdl	bdl	bdl	145.2	bdl	602.9
Shuiyindong	Opy + PrePy1	34332-44 at 33.28 g/t	373,606.8	bdl	bdl	bdl	115.0	116.7	735.7
Jinfeng	Opy + PrePy1	HDDS0154B-767 at 91.7 g/t	677,296.3	46.6	195.5	395.8	108.6	196.2	1,075.3
Shuiyindong	Opy + PrePy2	SYD-2F-4 at 77.2 g/t	561,742.7	bdl	bdl	156.7	132.8	1,420.1	292.8
Shuiyindong	Opy + PrePy2	SYD-2F-4 at 77.2 g/t	418,821.7	bdl	bdl	57.2	29.4	630.1	46.8
Shuiyindong	Opy + PrePy2	SYD-3A-1 at 31.9 g/t	624,508.9	bdl	bdl	bdl	51.6	353.2	660.0
Shuiyindong	Opy + PrePy2	SYD-3A-1 at 31.9 g/t	443,818.4	82.4	bdl	bdl	78.7	124.2	1,882.2
Shuiyindong	Opy + PrePy2	34332-45 at 3.56 g/t	557,434.9	bdl	bdl	105.6	270.4	bdl	248.2
Shuiyindong	Opy + PrePy2	34332-45 at 3.56 g/t	650,673.5	bdl	bdl	74.7	607.4	bdl	318.7
Shuiyindong	Opy + PrePy2	34332-45 at 3.56 g/t	715,501.1	bdl	33.0	75.4	331.4	254.5	196.6
Jinfeng	Opy + PrePy2	HDDS0154B-766 at 57 g/t	625,588.5	bdl	107.4	bdl	bdl	bdl	bdl
Jinfeng	Opy + PrePy2	HDDS0154B-766 at 57 g/t	560,645.2	bdl	bdl	bdl	60.2	344.1	141.5
Jinfeng	Opy + PrePy2	HDDS0154B-767 at 91.7 g/t	626,470.6	64.9	bdl	bdl	82.4	701.1	1,170.5
Jinfeng	Opy + PrePy2	HDDS0091-507 at 28.4 g/t	444,660.5	bdl	139.7	bdl	bdl	439.6	1,225.0
Jinfeng	Opy + PrePy2	HDDS0091-507 at 28.4 g/t	363,877.7	bdl	bdl	bdl	71.7	398.8	1,971.6

Abbreviations: bdl = below detection limit, OPy = ore pyrite, PrePy1 = pre-ore pyrite 1, PrePy2 = pre-ore pyrite 2, PrePy3 = pre-ore pyrite 3, PrePy4 = pre-ore pyrite 4

APPENDIX 2. *(Cont.)*

Deposit	Zn	As	Se	Mo	Ag	Cd	Sn	Sb	Au	Hg	Tl	Pb	Bi
Shuiyindong	bdl	1,723.6	bdl	45.9	bdl	bdl	bdl	74.0	46.6	33.9	21.5	67.2	bdl
Shuiyindong	234.9	919.6	bdl	bdl	17.8	bdl	bdl	49.8	6.5	91.9	14.7	151.0	bdl
Shuiyindong	1,426.5	10,394.6	bdl	bdl	bdl	bdl	28.1	177.7	702.2	54.8	65.4	41.0	bdl
Shuiyindong	bdl	1,514.3	bdl	bdl	bdl	bdl	bdl	39.7	92.1	36.6	10.9	97.3	bdl
Shuiyindong	bdl	4,385.9	bdl	81.1	bdl	bdl	bdl	132.2	49.1	bdl	22.5	74.8	bdl
Jinfeng	495.3	15,516.6	bdl	bdl	13.6	bdl	bdl	508.5	688.1	48.9	bdl	361.9	15.2
Shuiyindong	bdl	11,264.0	bdl	bdl	bdl	bdl	bdl	159.8	23.9	22.6	12.6	115.1	bdl
Shuiyindong	bdl	7,349.5	bdl	bdl	bdl	bdl	bdl	129.8	19.7	bdl	11.8	75.1	bdl
Shuiyindong	438.4	16,927.9	bdl	38.2	bdl	bdl	bdl	43.3	219.3	22.0	bdl	27.3	bdl
Shuiyindong	bdl	10,600.6	bdl	bdl	16.1	bdl	bdl	198.6	1,158.4	bdl	19.5	62.9	bdl
Shuiyindong	279.7	99.0	bdl	bdl	bdl	bdl	20.8	5.7	3.2	bdl	bdl	bdl	bdl
Shuiyindong	261.4	2,335.3	bdl	bdl	7.6	bdl	45.3	141.2	4.5	110.3	60.3	90.9	7.4
Shuiyindong	bdl	63.5	bdl	bdl	bdl	bdl	bdl	16.0	2.9	bdl	bdl	184.7	4.1
Jinfeng	bdl	6,743.9	bdl	bdl	bdl	bdl	bdl	109.1	11.0	bdl	bdl	125.2	bdl
Jinfeng	247.8	3,587.4	bdl	bdl	bdl	bdl	bdl	139.1	54.9	54.5	7.8	115.6	bdl
Jinfeng	bdl	24,887.3	bdl	27.2	9.8	149.3	bdl	797.6	384.7	123.0	45.3	611.0	9.4
Jinfeng	976.9	1,936.0	bdl	bdl	bdl	bdl	66.3	404.5	17.1	bdl	bdl	393.1	15.0
Jinfeng	295.5	5,805.5	bdl	bdl	19.3	bdl	bdl	296.8	27.0	146.6	11.8	280.5	5.4

SCIENTIFIC COMMUNICATIONS

APPENDIX 3

Spearman Rank Correlation Matrix of Major and Trace Elements in Shuiyindong and Jinfeng Ore Pyrite from LA-ICP-MS Analyses

	S	V	Cr	Mn	Co	Ni	Cu	Zn	As	Se	Mo	Ag	Cd	Sn	Sb	Au	Hg	Tl	Pb
V	-0.01																		
Cr	0.05	0.14																	
Mn	-0.08	0.25	0.19																
Co	0.04	-0.03	-0.06	0															
Ni	0.17	-0.04	-0.05	-0.04	0.18														
Cu	-0.34	0.02	0.13	-0.06	-0.08	-0.18													
Zn	0.07	-0.07	0.1	0.13	-0.02	-0.02	-0.03												
As	0.4	0.1	0.11	-0.05	-0.19	-0.01	0.03	0.15											
Se	0.08	0.01	-0.06	-0.05	-0.03	-0.05	-0.01	-0.07	-0.07										
Mo	0.06	0.05	-0.11	0.26	-0.03	-0.08	-0.1	0.12	0.03	-0.05									
Ag	0.06	-0.05	0.03	-0.04	0.09	0.11	0.11	-0.12	0.04	-0.02	-0.01								
Cd	0.15	-0.06	-0.05	-0.06	**0.51**	0.06	-0.03	0.08	-0.01	0.23	-0.03	0.07							
Sn	0.09	-0.03	0.06	-0.07	0.01	0.08	-0.03	0.11	-0.04	-0.03	-0.04	0.1	-0.08						
Sb	0.17	0.13	0.1	-0.02	-0.01	-0.04	0.09	0.14	**0.53**	-0.07	-0.01	0.21	0.01	0.15					
Au	0.15	0.09	0.1	0.03	-0.1	-0.28	0.24	0.02	**0.52**	-0.09	0.05	0.23	0.01	-0.06	**0.6**				
Hg	0.1	-0.01	-0.05	-0.06	0.05	-0.07	-0.1	0.11	0.33	0	-0.03	0.24	0.04	-0.01	**0.65**	0.31			
Tl	0.05	-0.01	0.04	-0.06	0.1	-0.06	0.07	0.15	0.34	-0.04	-0.06	0.13	0.17	0.06	**0.65**	**0.55**	**0.44**		
Pb	0.24	0.07	0.03	-0.06	0.25	0.09	-0.06	0.24	**0.42**	-0.07	0.01	0.09	0.16	0.2	**0.8**	0.26	**0.53**	**0.46**	
Bi	0.19	0.04	0.16	0.06	-0.03	0.07	0.03	0.24	0.18	-0.01	-0.06	0.14	0.01	0.13	0.23	0.04	0.11	0.11	0.37

Values >0.4 and <–0.4 are in bold; number of ore pyrite analyses = 109: 70 analyses from Shuiyindong and 39 analyses from Jinfeng; complete LA-ICP-MS data are included in Appendix 2

Zhuojun Xie graduated from Chang'an University with a B.A. degree in mineral resource exploration engineering in 2011, and from the University of Chinese Academy of Sciences with a Ph.D. degree in economic geology in 2016. From September 2014 to January 2016, he worked with Prof. Jean Cline at the University of Nevada, Las Vegas as a joint-training Ph.D. student. He began his career at the Institute of Geochemistry, Chinese Academy Sciences as an assistant research professor starting in August 2016. His most recent research has focused on Carlin-type Au deposits in Guizhou Province, China, and Nevada, USA.